sustainability

MDPI

Article

Winter and Summer $PM_{2.5}$ Land Use Regression Models for the City of Novi Sad, Serbia

Sonja Dmitrašinović [1], Jelena Radonić [1], Marija Živković [2], Željko Ćirović [2], Milena Jovašević-Stojanović [2] and Miloš Davidović [2,*]

[1] Faculty of Technical Sciences, University of Novi Sad, Trg Dositeja Obradovića 6, 21000 Novi Sad, Serbia; dmitrasinovic@uns.ac.rs (S.D.); jelenaradonic@uns.ac.rs (J.R.)
[2] VIDIS Centre, "Vinča" Institute of Nuclear Sciences, National Institute of the Republic of Serbia, University of Belgrade, Mike Petrovića Alasa 12-14, 11000 Belgrade, Serbia; marijaz@vin.bg.ac.rs (M.Ž.); zeljko.cirovic@vin.bg.ac.rs (Ž.Ć.); mjovst@vin.bg.ac.rs (M.J.-S.)
* Correspondence: davidovic@vin.bg.ac.rs

Abstract: In this study, we describe the development of seasonal winter and summer (heating and non-heating season) land use regression (LUR) models for $PM_{2.5}$ mass concentration for the city of Novi Sad, Serbia. The $PM_{2.5}$ data were obtained through an extensive seasonal measurement campaign conducted at 21 locations in urban, urban/industrial, industrial and background areas in the period from February 2020–July 2021. At each location, $PM_{2.5}$ samples were collected on quartz fibre filters for 10 days per season using a reference gravimetric pump. The developed heating season model had two predictors, the first can be associated with domestic heating over a larger area and the second with local traffic. These predictors contributed to the adjusted R^2 of 0.33 and 0.55, respectively. The developed non-heating season model had one predictor which can be associated with local traffic, which contributed to the adjusted R^2 of 0.40. Leave-one-out cross-validation determined *RMSE*/mean absolute error for the heating and non-heating season model were 4.04/4.80 μg/m^3 and 2.80/3.17 μg/m^3, respectively. For purposes of completeness, developed LUR models were also compared to a simple linear model which utilizes satellite aerosol optical depth data for $PM_{2.5}$ estimation, and showed superior performance. The developed LUR models can help with quantification of differences between seasonal levels of air pollution, and, consequently, air pollution exposure and association between seasonal long-term exposure and possible health risk implications.

Keywords: fine particulate matter; land use regression (LUR); heating/non-heating seasonal $PM_{2.5}$ model; digital twin; aerosol optical depth

check for updates

Citation: Dmitrašinović, S.; Radonić, J.; Živković, M.; Ćirović, Ž.; Jovašević-Stojanović, M.; Davidović, M. Winter and Summer $PM_{2.5}$ Land Use Regression Models for the City of Novi Sad, Serbia. *Sustainability* **2024**, *16*, 5314. https://doi.org/10.3390/su16135314

Academic Editor: David Lopez-Carr

Received: 27 March 2024
Revised: 12 June 2024
Accepted: 13 June 2024
Published: 21 June 2024

Copyright: © 2024 by the authors. Licensee MDPI, Basel, Switzerland. This article is an open access article distributed under the terms and conditions of the Creative Commons Attribution (CC BY) license (https://creativecommons.org/licenses/by/4.0/).

1. Introduction

Particulate matter pollution is known to be the single largest environmental health risk in Europe [1] and various adverse health effects are linked to the exposure to particulate matter (PM) [2,3]. With the continuous rapid growth of urban areas, dense air quality monitoring within these environments becomes increasingly important since significant contrasts in ambient air quality and level of $PM_{2.5}$ can exist within different city microenvironments and consequently manifest different degree of health risks [4,5].

However, sparse referent monitoring networks and limited geographic coverage, which makes capturing intra-city variabilities difficult, are the reality of most countries in the world [6]. Nowadays there is a wide palette of different techniques used for processing air quality data with the goal of estimating spatial variations in measured pollutants, and assessing exposure, each having different requirements for data availability, going from more simple spatial interpolation methods to the more advanced dispersion models that integrate chemical transport modelling.

Data-driven statistical modelling of air pollution generally has several advantages in the specific context of land use regression (LUR) modelling. LUR modelling has a solid foundation since it relies on directly measuring air pollution using typical reference instruments, and it allows for approximate modelling of pollution sources/sinks or their proxies on both smaller and larger scales of spatial variation but does so without introducing complexities of the physical–chemical modelling and dependencies of extensive datasets. This makes, in a way, LUR models robust and capable of quantifying the level of air pollution and air pollution exposure even at the personal level [6–19]. Many LUR models were developed for densely populated cities where high levels of air pollution were detected. Those studies focused on the development of either local or regional LUR models [20–22]. A well-known LUR model targeting multiple European cities was developed in the framework of the European Study of Cohorts for Air Pollution Effects—ESCAPE project [14,23,24]. The most commonly used target variables for LUR modelling in the context of air pollution are the $PM_{2.5}$ fraction of particulate matter pollution, and the concentration of gaseous pollutant, NO_2 [25]. These models can often provide a high percentage of explained variability. Recent publications that utilized LUR models for predicting $PM_{2.5}$ have implemented different advanced machine learning algorithms, satellite data or other approaches in combination with basic LUR modelling principles in order to enhance model prediction efficiency and ability to be used for a larger study area [15,17,18,26–32].

Monitoring air pollutants for LUR development is often time-limited to several sampling campaigns during the year, lasting one or two weeks [33–35]. Seasonal $PM_{2.5}$ LUR models have been developed in Asia [36], Canada [37], Iran [38] and Colombia [34]. Previously, in Serbia, adaptations of the European LUR model developed by Wang et al. in 2014 within the ESCAPE study [24] and its validation with the development of supporting average daily traffic intensity models, and data fusion simulation were performed in Belgrade for $PM_{2.5}$ by Davidović et al. [39] and for NO_2 by Davidović et al. [40]. Some aspects of the application of the European LUR model developed by Wang et al. [24] in the Novi Sad municipality were shown by Dmitrašinović et al. [41]. LUR models are usually developed based on 20–80 sites [24]; however, in the ESCAPE project, 40–80 and 20–40 sites in 36 study areas in Europe were used for NO_X and $PM_{2.5}$ model development [42]. The smaller the number of measurement sites used for assessing the level of pollutant concentration, the more the accuracy of the developed LUR model will depend on the position of the individual measuring points [43].

LUR model development typically has the following components: the target variable specifications (specific air quality measurements (e.g., NO_2, $PM_{2.5}$) we want to predict or estimate), specific air pollution campaign data or existent air pollution monitoring network data, land use and land cover maps (e.g., forests, residential areas, roads within the study area), distance to feature/buffer zones (used to model the correlations those features have with pollutant concentrations at a specific location), and other predictor variables [44]. Once a statistically significant relationship between predictor variables and a target pollutant is established, this relationship can be used to estimate pollutant concentrations at various unmonitored sites. This is possible as long as all the predictor variables can be calculated for those sites [18,26,31,44–46].

In this study, we had a goal to develop seasonal winter and summer (heating and non-heating season) $PM_{2.5}$ land use regression (LUR) models for the city of Novi Sad, Serbia. One of the main motivations behind such a modelling effort is filling in the knowledge gap on spatial and seasonal variations in $PM_{2.5}$ concentrations since the network of reference monitoring stations in the city is rather unevenly distributed. In addition, in most cities in Serbia, PM concentrations show drastic differences in heating and non-heating seasons, thus the origin and quantification of this potential difference in the city of Novi Sad needs confirmation. Once in place, these models can help with the quantification of the level of air pollution, air pollution exposure, and the association between long-term exposure and various health risks, even in microenvironments not covered by regulatory monitoring.

Furthermore, these models can also be used to obtain high-resolution seasonal base maps for $PM_{2.5}$ concentrations in the city of Novi Sad.

2. Materials and Methods

2.1. Study Area

Novi Sad, Serbia's second largest city after the capital, Belgrade, is an urban-industrial agglomeration divided by the Danube River into two distinct regions. The city encompasses an area of 702.7 km^2 and experiences a regional climate that transitions from moderately continental to continental. Novi Sad sits at an elevation of approximately 80 m above sea level [47]. According to the latest publicly available population census data from 2022 [48], the city has 367,121 inhabitants.

Urban air quality in Novi Sad is influenced by several factors, including residential heating using wood, coal or natural gas, intensive traffic in urban areas, low energy efficiency of plants in the energy sector and industry, diffuse pollution from agriculture, and others [49]. Fine particulate matter pollution in Novi Sad frequently exceeds the proposed daily and annual WHO limits of 15 $\mu g/m^3$ and 5 $\mu g/m^3$, respectively [50]. In Novi Sad, $PM_{2.5}$ is measured by two networks, the national network running under the Serbian Environmental Protection Agency (SEPA) (one measuring site, urban) and a local network established by the City Administration for Environmental Protection (two measuring sites, urban and industrial) [51]. The study area and sampling sites were categorized into urban zone (URB), industrial zone (IND), border of urban and industrial zone (URB/IND) and background zone (BCG). Figure 1 shows a photo of each of the sampling location types.

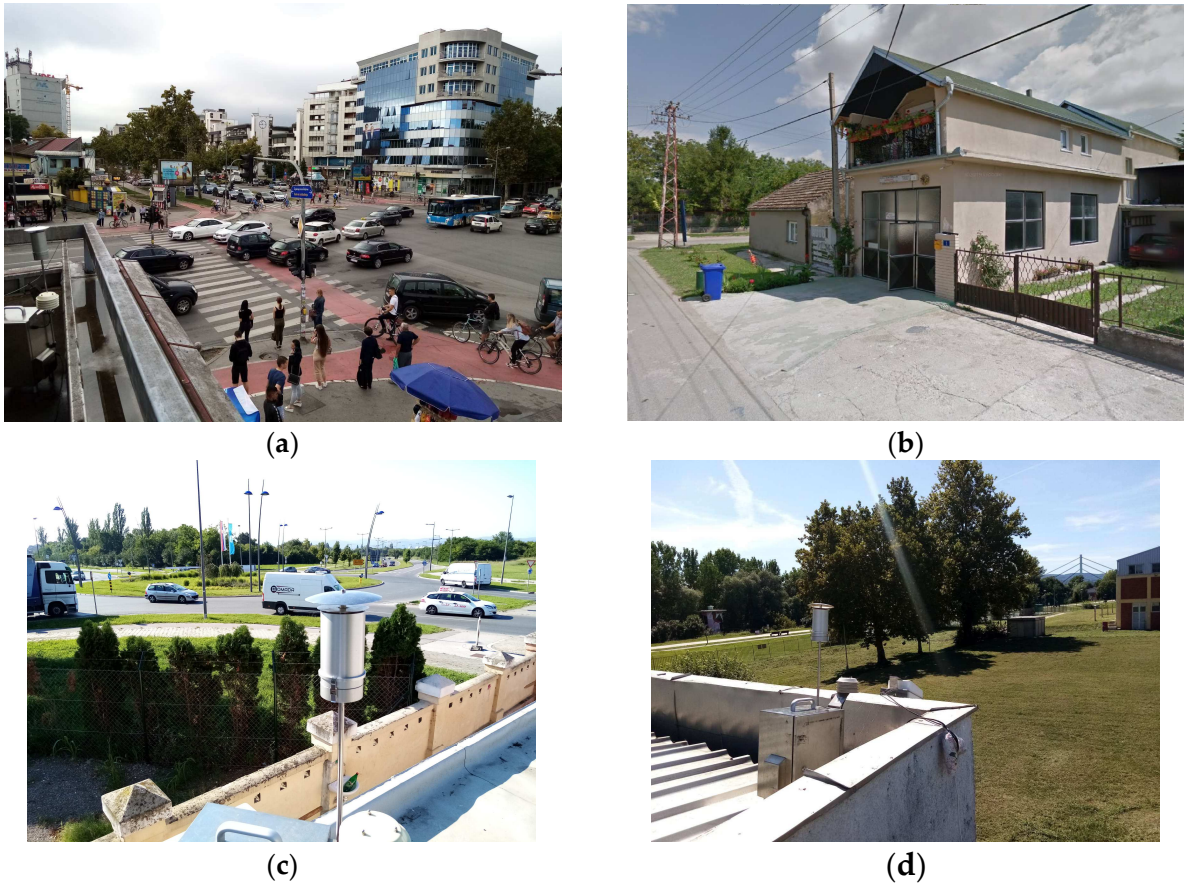

Figure 1. Example of measuring sites: (**a**) site 13 in the urban zone, (**b**) site 3 at the border of the urban and industrial zone, (**c**) site 7 in the industrial zone and (**d**) site 17 in the background zone. Table 1 provides more details on each of the measuring sites.

Table 1. Locations used for $PM_{2.5}$ sampling in two seasons: location types, coordinates and sampling periods.

Location Number	Measuring Location	Coordinates		Location Type/Traffic Type/Heating Type Options	Sampling Period
		Latitude	Longitude		
1	Veselina Maslese	45.26928	19.83304	URB/vicinity of roundabout, traffic site/DH area	8 September–18 September 2020 8 December–18 December 2020
2	Temerinski put	45.29313	19.83101	URB/traffic site/IH area	26 January–5 February 2021 6 July–16 July 2021
3	Svetozara Savkovica	45.28565	19.82087	URB, IND/resident area, low traffic/IH area	15 February–25 February 2020 24 July–3 August 2020
4	Sopocanska	45.26471	19.83378	URB/resident area, low traffic/IH area	26 February–7 March 2020 4 August–14 August 2020
5	Sirine I	45.22417	19.86177	URB/resident area, low traffic/IH area	8 September–18 September 2020 26 December 2020–5 January 2021
6	Save Ljubojeva	45.26074	19.7998	URB/strict resident area, no traffic/DH area	26 February–7 March 2020 4 August–14 August 2020
7	Rumenacki put	45.24968	19.82467	IND/high traffic site, vicinity of roundabout/IH area	8 March–18 March 2020 15 August–25 August 2020
8	Rackog	45.23406	19.88453	URB/traffic site/IH area	15 February–25 February 2020 24 July–3 August 2020
9	Pavla Ivica	45.25226	19.83725	URB/resident area, low traffic/DH area	4 August–14 August 2020 11 January–21 January 2021
10	Partizanska	45.24932	19.87728	URB/traffic site/IH area	8 September–18 September 2020 8 December–18 December 2020
11	Mise Dimitrijevica	45.24814	19.83448	URB/traffic site/DH area	15 February–25 February 2020 24 July–3 August 2020
12	Juraja Krizanica	45.27573	19.80066	URB/traffic site/IH area	8 March–18 March 2020 15 August–25 August 2020
13	Jevrejska	45.22818	19.89271	URB/high traffic site, vicinity of intersection/DH area	26 August–5 September 2020 11 January–21 January 2021
14	Janka Cmelika	45.26472	19.80861	URB/traffic site, low traffic/DH area	15 February–25 February 2020 24 July–3 August 2020
15	Hajduk Veljkova 4	45.24167	19.80375	URB/traffic site, vicinity of intersection/border of DH and IH area	8 March–18 March 2020 15 August–25 August 2020
16	Hajduk Veljkova 11	45.25749	19.8238	URB/traffic site/DH area	8 September–18 September 2020 9 February–19 February 2021

Table 1. *Cont.*

Location Number	Measuring Location	Coordinates		Location Type/Traffic Type/Heating Type Options	Sampling Period
		Latitude	Longitude		
17	Jirecekova	45.26078	19.80913	BCG/vicinity of the river, no traffic/DH area	26 August–5 September 2020 8 December–18 December 2020
18	Darinke Grujic	45.24124	19.85262	URB/residential area, low traffic/IH area	26 August–5 September 2020 8 December–18 December 2020
19	Bulevar PP	45.23936	19.78643	URB/traffic site/border of DH area and IH area	8 March–18 March 2020 15 August–25 August 2020
20	Beogradski kej	45.25608	19.85465	URB/traffic site/DH area	26 January–5 February 2021 6 July–16 July 2021
21	Balzakova	45.23787	19.83439	URB/residential area, low traffic/DH area	26 February–7 March 2020 4 August–14 August 2020

2.2. Sampling Campaign

The sampling campaign was conducted during winter (15 February–18 March 2020, 8 December 2020–19 February 2021) and summer (24 July–18 September 2020, 6–16 July 2021) periods and $PM_{2.5}$ was measured at 21 locations. At each location, $PM_{2.5}$ was collected for 10 days using a reference gravimetric pump Sven Leckel Model LVS3, with standard $PM_{2.5}$ inlet and 2.3 lpm flow rate. Gravimetric pumps were set to sample air for 48 h and collect particles on quartz fiber filters (Whatman QM-A, 47 mm). We had a total of 4 gravimetric pumps, thus particle concentrations during the winter and summer seasons were collected in batches of 4 sites simultaneously, for 10 days at each site per season. Each sample was collected for 48 h, resulting in 5 samples at each site per season. This cycle was performed until all measurements were completed at all 21 sites. Based on these results, seasonal averages were calculated according to the ESCAPE exposure manual [52].

Figure 2a shows 21 measuring locations, divided by colour according to type (URB, IND, BCG, URB/IND). Of these locations, 18 can be classified as URB-type locations with different levels of traffic intensity. During the heating season, air quality strongly depends on heating modalities present in urban microenvironments (individual heating (IH) using wood, coal, gas and electricity, or district heating by thermal power plants (DH), see Table 1). Location no. 7 is in the IND zone, location no. 3 is on the very border of the URB/IND zone, and location no. 17 is in the vicinity of the local background station, thus it is treated as a BCG site. The background location is situated near the Danube River, a residential area heated by a DH and near a pedestrian zone, with no traffic or domestic heating nearby. In Figure 2b, DH area borders and *coverage* areas (orange, pink, blue, and yellow colour) are shown and every study site is numbered (from 1–21), following the site sequence given in Table 1. Sampling sites are coloured green and white, that is, sites marked with the green colour are within areas that are within the city DH area, and sites marked with the white colour, are within areas with mixed means of individual heating (denoted as IH area in subsequent text).

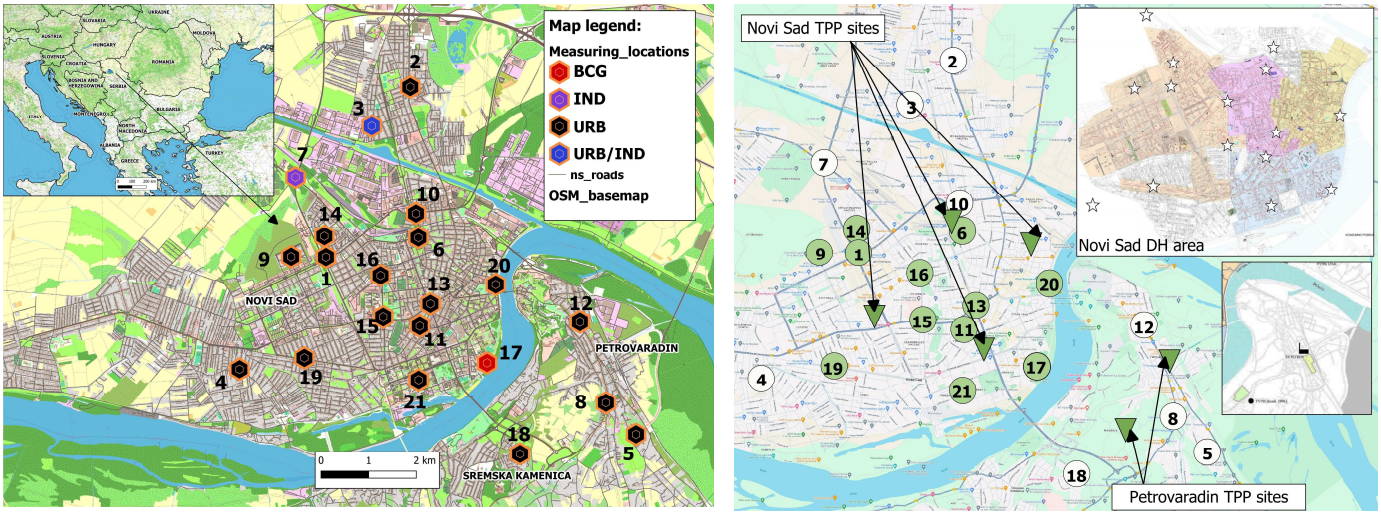

(**a**) (**b**)

Figure 2. (**a**) Map of the background (BCG), industrial (IND), urban (URB) and urban/industrial (URB/IND) sampling sites in Novi Sad used for developing the seasonal LUR models. (**b**) City Thermal power plant (TPP) sites (green triangle) and district heating (DH) area borders (figure inset). Numbering of sampling sites corresponds to Table 1.

2.3. Model Development and Evaluation

The database containing all $PM_{2.5}$ measurements from the 21 sites and a set of potential predictor variables was used for LUR model development. ESCAPE methodology [24,38,53,54] was applied, including enforcement of potential predictor direction of effect, as listed in Table A1. The initial step in model development was calculating univariate regression between each potential predictor variable (Table A1) and measured $PM_{2.5}$ target variable (Table 2) in order to determine the strength of their correlation by observing the Pearson correlation coefficient (R) and p-value. The predictor variable with the highest R value was used in the model, and the supervised stepwise forward procedure was continued in an iterative manner. Predictor variables that were not correlated with $PM_{2.5}$ measurements, had $p > 0.05$, did not have all observations for the study sample ($N = 21$) or had a predictor direction of effect opposite to the initially defined direction of effect were rejected. Additionally, for the buffer type predictor variables, if in the set of variables (e.g., corresponding to road length variable *ROADLENGTH_50m*) one had the highest correlation with $PM_{2.5}$, then the variable with the smaller buffer radius was not considered since values of this variable were already included within the larger buffer (e.g., variable *ROADLENGTH_25m* was not taken into account since the larger buffer, variable *ROADLENGTH_50m*, is included). One other criterion was if, e.g., variable *ROADLENGTH_100m* also had a significant correlation with $PM_{2.5}$, then in the regression model, an additional ring buffer was defined as the difference between *ROADLENGTH_100m* and *ROADLENGTH_50m*. After all remaining suitable predictor variables were added one by one into the set of possible predictor variables, the change in the percentage of explained variance of $PM_{2.5}$ (*adjusted* R^2, *adj.* R^2) was observed. During the stepwise iterative procedure for the LUR model development, the following steps were followed in order to avoid overfitting and to ensure the choice of a stable model. In each step, the best candidate predictor is included in the model only if the adjusted R^2 increased by more than 1%, otherwise, if there is no such predictor, the iterative procedure stops and the model is finalized. The direction of effect (i.e., sign of the coefficient corresponding to the particular predictor) for the newly included predictor must be in accordance with the predetermined sign, and furthermore, all coefficients in the new regression equation must remain the same, i.e., in accordance with their predetermined direction of effect [53]. Adding predictors to the model stops when there are no remaining predictors that can

increase *adj.* R^2 by at least 1% compared to the previous regression model. As a final step, variables that are not statistically significant ($p > 0.10$), were eliminated from the model, while those with $p \leq 0.10$ were kept in the model.

Table 2. Mean seasonal $PM_{2.5}$ concentrations ($\mu g/m^3$) for all sites during heating and non-heating seasons.

Site No.	Location Type	Winter $PM_{2.5}$	Summer $PM_{2.5}$
1	URB	25.57	19.56
2	URB	50.21	22.31
3	URB/IND	43.77	14.22
4	URB	38.19	10.85
5	URB	34.17	10.49
6	URB	32.89	10.71
7	IND	39.65	17.14
8	URB	33.55	13.72
9	URB	25.25	12.19
10	URB	35.64	20.36
11	URB	25.45	22.48
12	URB	36.81	13.73
13	URB	34.16	20.62
14	URB	27.92	16.15
15	URB	35.63	14.41
16	URB	28.37	17.82
17	BCG	27.39	12.22
18	URB	32.5	16.15
19	URB	36.12	14.81
20	URB	30	20.32
21	URB	26.2	10.47

Note. URB—urban location, IND—industrial location, URB/IND—location at the border of the urban and industrial zone, BCG—background location.

Evaluation of the final winter and summer $PM_{2.5}$ LUR models was conducted by examining Cook's distance (Cook's D), heteroscedasticity (White test) and normality of residual distribution.

For model validation, we used the Leave-One-Out Cross-validation (LOOCV), in which data from one site is left out, the LUR model is rebuilt based on the remaining points, the error for the left-out point is calculated, and then the total error is averaged for all observation sites. The benefit of such a leave-one-out analysis is that, in a way, all measuring points are used for both model development and model validation. The performance of the developed model was assessed by observing *adj.* R^2, *RMSE* and *MAE* values [38,54,55].

3. Results

3.1. $PM_{2.5}$ Measurements

Mean seasonal $PM_{2.5}$ concentrations during heating and non-heating seasons and their descriptive statistics are given in Tables 2 and 3. Note that, as mentioned in the Materials and Methods section, each location had a total of five 48 h measurements per season that were used for inferring seasonal concentrations. Some details and comments about these individual measurements are stated in Appendix D.

Table 3. $PM_{2.5}$ ($\mu g/m^3$) descriptive statistics for heating and non-heating seasons.

Statistics	Winter $PM_{2.5}$	Summer $PM_{2.5}$
Median	33.55	14.81
Mean	33.31	15.75
Std. Deviation	6.44	3.99
Minimum	25.25	10.47
Maximum	50.21	22.48
Variance	41.43	15.92

3.2. Development and Evaluation of Seasonal LUR Models

3.2.1. Development and Evaluation of Winter LUR Model

Among all the potential predictor variables offered for the development of the winter $PM_{2.5}$ LUR model ($PM_{2.5}$_LUR_{WINTER}) from Table A1, variables *ROADLENGTH_50m*, *park_area_3000m*, *suburban_area_3000m*, *class3_area_1000m* and *resident_area_300m* had the highest R; however, *class3_area_1000m* and *resident_area_300m* were not used in further calculation due to insufficient number of observations (different from zero). Correlations between $PM_{2.5}$ and potential predictors expressed through the *R* values and the number of observations for these potential predictors are given in Table 4.

Table 4. Correlation coefficient, *R*, and the number of available observations (different from zero), *N*, for the initial set of possible predictors for the winter LUR model.

Predictors	*R*	*N*
ROADLENGTH_50m	0.458 *	21
Class3_1000m	−0.778 *	7
park_area_3000m	−0.548 *	21
suburban_area_3000m	0.602 **	21
resident_area_300m	0.497 *	18

The distinction between moderate and strong correlations was made based on *p*-value using the following criteria: $p < 0.05$ (moderate correlation, marked by *), and $p < 0.01$ (strong correlation, marked by **).

Tested models considered within a forward stepwise regression process along with values of R^2, *adj.* R^2, *F*-test, *DF*, *p*-value, *VIF* and *RMSE* are given in Table 5. Considering the values of *adj.* R^2 and *RMSE*, the third model in which the predictor variables are *suburban_area_3000m* and *ROADLENGTH_50m* is noticeably better than the first and second proposed models, and as such it is optimal for predicting winter $PM_{2.5}$. The values of *B* (unstandardized) coefficient and the *p*-value for optimal model final predictors are $B = 0.0000019$, $p = 0.001$ for suburban_area_3000m and $B = 0.024$, $p < 0.01$ for *ROADLENGTH_50m*. Unstandardized coefficients in the final regression equations are used due to different measuring scales of predictors. The *VIF* criteria for multicollinearity and Cook's D criteria used for model development were <3 and <1 [56].

Table 5. Models tested for the winter season.

Potential Predictors	*R*	*adj.* R^2	*F*-Test	*DF*	*p* Value	*VIF*	*RMSE*
suburban_area_3000m	0.602	0.328	10.77	1. 19	0.004	1.00	5.02
suburban_area_3000m+park_area_3000m	0.624	0.322	5.75	2. 18	0.012	2.05	4.91
suburban_area_3000m+ROADLENGTH_50m	**0.770**	**0.548**	**13.12**	**2. 18**	**0.000**	**1.00**	**4.01**

Note. *R*—coefficient of multiple correlation, *adj.* R^2—corrected coefficient of multiple determination—percentage of explained variance, *F*-Test—value of the *F* quotient, *DF*—number of degrees of freedom, *VIF*—variance inflation factor (multicollinearity index), *RMSE*—root mean square error.

The regression equation for this final $PM_{2.5}$_LUR_{WINTER} model is given by Equation (1). By applying the final $PM_{2.5}$_LUR_{WINTER} regression formula, it is possible to explain about 55% of the variance in the $PM_{2.5}$ concentration.

$$PM_{2.5}_LUR_{WINTER} = 24.89 + suburban_area_3000m \times 1.9 \times 10^{-6} + ROADLENGTH_50m \times 2.4 \times 10^{-2} \quad (1)$$

The evaluation process for the model gave Cook's D observation values below 1 and White's test was not statistically significant ($\chi^2(5) = 1.21$, $p = 0.944$), with a p-value higher than the level of significance (0.05) [57], showing the absence of heteroscedasticity from the tested data (Figure 3b). Values of skewness ($SK = -0.077$) and kurtosis coefficients ($KU = -1.09$) are within the acceptable range ± 1 [58,59], thus the distribution of residuals for the winter model can be treated as near normal as presented on residual plots in Figure 3a–d.

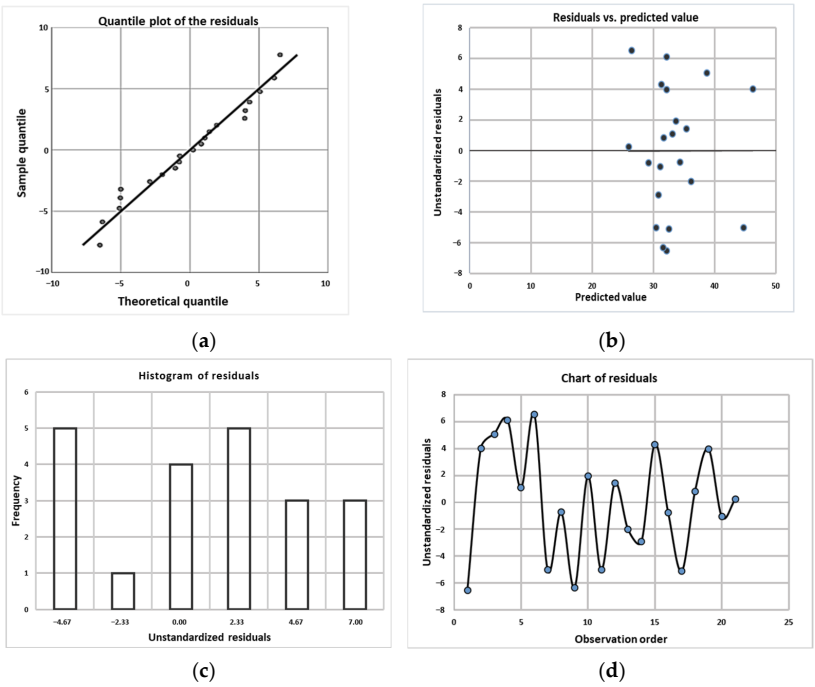

Figure 3. Residual plots for winter: (**a**) Quantile plot of the residuals; (**b**) Residuals vs. predicted values; (**c**) Histogram of the residuals; (**d**) Chart of residuals.

Validation of the model using LOOCV is presented in Appendix B.

3.2.2. Summer LUR Model Development and Evaluation

For the development of a summer LUR model ($PM_{2.5}_LUR_{SUMMER}$), all potential predictor variables, their correlations with target $PM_{2.5}$ expressed through their R values and the number of observations are shown in Table 6. The same elimination criteria used in the winter model were applied to these potential predictors. Buffer-type predictor variables that significantly correlate with the $PM_{2.5}$ but also have a corresponding predictor with a smaller buffer radius that has a lower correlation were not included in the model. For example, the variable *SECONDARYROADLENGTH_500m* was not included in the analysis as a predictor because the variable *SECONDARYROADLENGTH_1000m* is more strongly correlated to $PM_{2.5}$ and has a larger buffer radius. When a variable of the same class has a weaker correlation with the dependent $PM_{2.5}$ variable compared to the same class with a smaller buffer radius, then a new ring buffer variable is derived. For example, from the difference of variables *ROADLENGTH_300m* and *ROADLENGTH_50m*, the variable *ROADLENGTH_50_300* is considered for inclusion in the model.

Table 6. Correlation coefficient, *R*, and the number of available observations (different from zero), *N*, for the initial set of possible predictors for the summer LUR model.

Predictors	*R*	*N*
ROADLENGTH_25m	0.497 *	21
ROADLENGTH_50m	0.658 **	21
ROADLENGTH_100m	0.494 *	21
ROADLENGTH_200m	0.507 *	21
ROADLENGTH_500m	0.510 *	21
PRIMARYROADLENGTH_100m	0.951 *	4
PRIMARYROADLENGTH_200m	0.981 *	4
PRIMARYROADLENGTH_300m	0.994 **	4
PRIMARYROADLENGTH_500m	0.813 *	7
SECONDARYROADLENGTH_500m	0.574 *	16
SECONDARYROADLENGTH_1000m	0.680 **	21
SECONDARYROADLENGTH_1500m	0.479 *	21
DISTINVSECOND1	0.491 *	21
DISTINVSECOND2	0.442 *	21
Class2_300m	0.956 *	4
industrial_area_300m	0.970 *	4

The distinction between moderate and strong correlations was made based on *p*-value using the following criteria: $p < 0.05$ (moderate correlation, marked by *) and $p < 0.01$ (strong correlation, marked by **).

Tested models considered within a forward stepwise regression process are given in Table 7. According to the values of *adj.* R^2, *adj.* ΔR^2, *RMSE* and *VIF* coefficients, the third model, which included the predictor variables *SECONDARYROADLENGTH_1000m*, *ROADLENGTH_50m* and *ROADLENGTH_50_300*, was optimal. This model had lower *RMSE* and higher *adj.* R^2 values compared with the first two models, and multicollinearity was not present, as in the fourth model. The fifth model has a negative *adj.* ΔR^2 coefficient value (compared to the third model), while in the sixth and seventh models, there are B coefficient values that are not in accordance with the direction of effect. By applying the final step in model development, that is, statistical significance criteria, variables *ROADLENGTH_50_300* and *SECONDARYROADLENGTH_1000m* were removed from the $PM_{2.5}$_LUR_{SUMMER} model because their $p > 0.05$. Thus, in the third optimal model, *ROADLENGTH_50m* is the only significant predictor of the positive direction, with a B coefficient of 0.020 and $p < 0.01$.

Table 7. Tested models for the summer season.

Potential Predictors	*R*	*adj.* R^2	*F*-Test	*DF*	*p* Value	*VIF*	*RMSE*
SECONDARYROADLENGTH_1000m	0.680	0.435	16.38	1.19	0.001	1.00	2.85
SECONDARYROADLENGTH_1000m + ROADLENGTH_50m	0.767	0.542	12.83	2.18	0.000	1.38	2.50
SECONDARYROADLENGTH_1000m + ROADLENGTH_50m + ROADLENGTH_50_300	**0.797**	**0.570**	**9.85**	**3.17**	**0.001**	**1.81**	**2.35**
SECONDARYROADLENGTH_1000m + ROADLENGTH_50m + ROADLENGTH_50_300 + ROADLENGTH_300_500	0.812	0.574	7.73	4.16	0.001	3.89	2.27
SECONDARYROADLENGTH_1000m + ROADLENGTH_50m + ROADLENGTH50_300 + DISTINVSECOND1	0.797	0.544	6.95	4.16	0.002	1.84	2.35
SECONDARYROADLENGTH_1000m + ROADLENGTH_50m + SECONDARYROADLENGTH_1000_1500m	0.836	0.623	9.27	4.16	0.000	2.78	2.14
SECONDARYROADLENGTH_1000m + ROADLENGTH_50m + ROADLENGTH_50_300 + DISTINVSECOND_2_1	0.797	0.544	6.96	4.16	0.002	1.84	2.35

Note. R^2—coefficient of multiple correlation, *adj.* R^2—corrected coefficient of multiple determination—percentage of explained variance, *F*-test—value of the *F* quotient, *DF*—number of degrees of freedom, *VIF*—variance inflation factor (multicollinearity index), *RMSE*—root mean square error.

This final $PM_{2.5}$_LUR_{SUMMER} model was shown to be statistically significant (*F*-test = 14.49, $p = 0.001$), with the regression equation represented by Equation (2). By applying this regression equation, the predictor explained 40.3% of the variation in the summer $PM_{2.5}$ concentration.

$$PM_{2.5}_LUR_{SUMMER} = 12.43 + ROADLENGTH_50m \times 2.0 \times 10^{-2} \quad (2)$$

Evaluation of the $PM_{2.5}_LUR_{SUMMER}$ model also showed that there were no observations with Cook's distances greater than 1.00, that White's test was not statistically significant (χ^2 (2) = 3.28, p = 0.198) (Figure 4b) and that values of skewness (SK = 0.853) and kurtosis (KU = −0.803) coefficients were within the acceptable range of ±1 [58,59], implying near normal residual distribution as can be seen on the residual plots (Figure 4a–d).

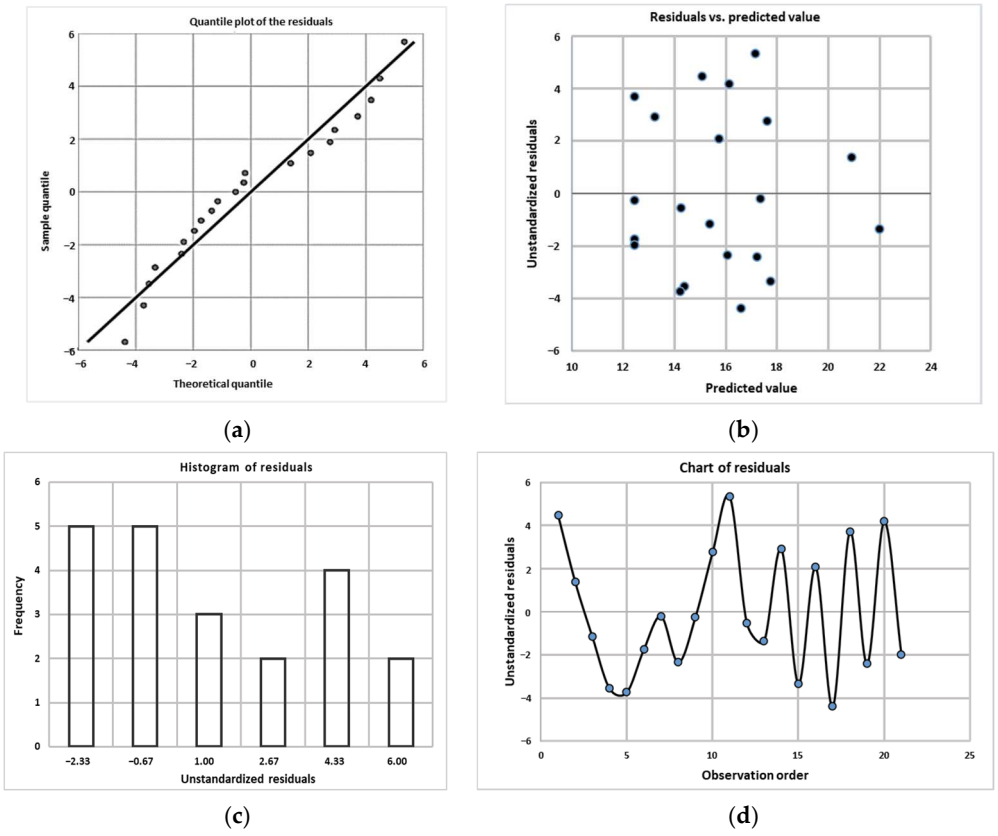

Figure 4. Residual plots for summer: (**a**) Quantile plot of the residuals; (**b**) Residuals vs. predicted values; (**c**) Histogram of the residuals; (**d**) Chart of residuals.

Validation of the model using LOOCV is described in Appendix B.

3.2.3. Simple Seasonal $PM_{2.5}$ Model Based on Aerosol Optical Depth Data

In this section, we show a simple and direct linear regression approach for connecting aerosol optical depth (AOD) data for the city of Novi Sad and $PM_{2.5}$ ground-level data.

In recent years, successful efforts have been made to utilize satellite-based aerosol information like observations of Aerosol Optical Depth (AOD) to improve the spatial mapping and prediction of ground-level $PM_{2.5}$. The relationship between AOD and PM is complex and depends on aerosol type and size, relative humidity, planetary boundary layer height and the vertical structure of aerosol distribution. Statistical approaches including single and multiple linear regression and more complex machine learning approaches for estimating PM based on satellite data have demonstrated some advantages compared to more traditional physical retrieval methods [60]. Various satellite products including Copernicus Atmosphere Monitoring Service (CAMS), Global Near-Real-Time provided by the European Centre for Medium-Range Weather Forecasts (ECMWF) [61] and MCD19A2.061: Terra & Aqua MAIAC Land Aerosol Optical Depth provided by NASA LP DAAC at the USGS EROS Center [62], can be used to infer ground level $PM_{2.5}$ concentrations using aerosol optical depth measurements originating from satellites. Such estimates of $PM_{2.5}$

can be conducted using statistical approaches, which can range in complexity from linear regression models (e.g., generalized linear model [63] multiple linear regression [64]) to more complex models based on machine learning approaches [65].

Google Earth Engine was used to access and process the ECMWF/CAMS and MODIS datasets. The spatial resolution of the CAMS data is approximately 0.1 degrees (~10 km at the equator), while the MODIS AOD data from the MCD19A2 product has a native spatial resolution of 1 km. The process involved filtering the data by date, selecting relevant bands for AOD, averaging the data over the specified periods and resampling the data using bilinear interpolation. Figure 5 shows a scatterplot and regression line for seasonal models that use simple univariate linear regression with no intercept to quantify the relation between AOD data and seasonal $PM_{2.5}$ ground-level data (which was also used for the seasonal LUR models presented in this paper). Validation of the model using the LOOCV approach is described in Appendix C.

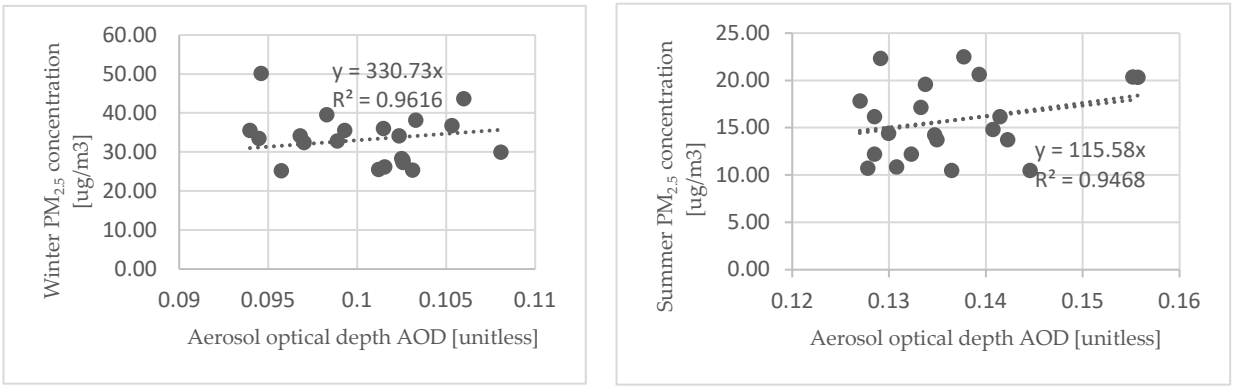

(**a**) (**b**)

Figure 5. Seasonal $PM_{2.5}$ concentration averages at 21 locations in the city of Novi Sad vs. aerosol optical depth (AOD) (**a**) during winter and (**b**) during summer.

4. Discussion

In most cities in Serbia, PM concentrations show drastic differences during heating and non-heating seasons [66], and the origin and simple quantification of this difference in the city of Novi Sad can be seen using results from reference monitoring and emission sources [67]; however, these lack spatial resolution. This difference was also analysed using a mobile monitoring approach (this increases spatial resolution) for PM_{10}, $PM_{2.5}$ and ultrafine aerosol fraction, and was performed using research-grade instruments, TSI Nanoscan 3910 and TSI OPS 3330 [68,69]. These underpinning reports and research studies gave motivation for the development of the seasonal LUR model, which used reference instruments and enables quantification of differences between seasonal levels of air pollution, and consequently air pollution exposure and association between seasonal long-term exposure and possible health risk implications over the whole city of Novi Sad.

The initial set of predictors for the development of the Novi Sad winter $PM_{2.5}$ LUR model (Table 4) had a mixture of source and sink predictors. The initial set contained the following predictors that model $PM_{2.5}$ sources: *ROADLENGTH_50m*, which is a proxy for traffic intensity on nearby roads; *suburban_area_3000m*, which can be used as a proxy for individual heating sources in a site's surrounding area, and similarly, *resident_area_300m*. The initial set contained the following $PM_{2.5}$ sinks: *Class3_1000m*, which is the number of forests and seminatural areas in a 1000 m buffer that models the amount of aerosol deposition, and similarly, *park_area_3000m*. Target $PM_{2.5}$ seasonal concentration was inferred based on the measuring campaign that was conducted during the heating season months from December to March. These raw measurements were corrected to obtain seasonal averages using the ESCAPE procedure [52].

The iterative development procedure resulted in the three models shown in Table 5. It is interesting to note that the best model in terms of explained variance contains only source predictors (*suburban_area_3000m*, *ROADLENGTH_50m*), while the second-best model contains a source (*suburban_area_3000m*) and a sink (*park_area_3000m*) predictor. While it is evident that the seasonal concentration depends on a complex interplay of source and sink processes, the extent of available data and applied statistical procedure for the model development favoured the source-only model.

The predictor group suburban area can be used as a proxy of air pollution sources related predominantly to household areas that are situated next to the urban city centre and DH area and quantifies the contribution of IH during the winter. The predictor that explained the most variance in $PM_{2.5}$ concentration during the winter season in Novi Sad was *suburban area in a buffer of 3000m*, with *adj.* R^2 = 0.328. Buffers with smaller radii did not show statistical significance when explaining $PM_{2.5}$ pollution. The second significant predictor variable, total road length within a buffer of 50 m, is a very rough proxy for variations in traffic density in the close vicinity, adding to the total explained variance of *adj.* R^2 = 0.548.

Generally, each developed LUR model contains unique definitions of potential independent variables, depending on the study area specifications, available data, and pollutants of interest [70]. In cases where data on traffic intensity are not available or do not exist and thus cannot be linked to the local and central road bases, road classification and their lengths within the research area can be used as proxies for the potential predictor variables [23,36,71]. Similarly, traffic emissions can be used as a proxy for major arterials, railroads or street lengths in cases where these data do not exist [72]. Seasonal LUR models that model higher winter concentrations of $PM_{2.5}$ and the potential influence of the heating combustion process were developed for several cities in China [35,73,74]. A winter model developed by Shi et al. [35] explained 61% of winter $PM_{2.5}$ variability, and predictors in the final LUR model were average building floor areas within 3000 m that explained the most variation, followed by water area within 3000 m and average building heights within 50 m (predictors with negative coefficients). Other types of predictors such as meteorological factors, roads, land use types, various points of interest for better temporal resolution and elevation were used for LUR model development in Beijing [73] and explained between 54–86% of $PM_{2.5}$ winter variability. The highest percentage of explained $PM_{2.5}$ variability among the mentioned heating season models was 94%, with the explanatory variables precipitation, density of roads, elevation, average air pressure and vegetation [74]. The LUR model created by Saucy et al. [75] explained 29% of the variance with the use of population/building density within 25 and 300 m buffers, construction sites within a 100 m buffer, length of bus routes in a 300 m buffer and distance to the nearest waste burning sites as explanatory variables. Road lengths, as significant predictors within smaller buffer zones, were also reported in winter LUR models developed for Calgary, Canada [37], where the total length of major roads within a buffer of 200 m was significant, noting that in that study buffer zones started from 100 m due to local city fabric. The value of adj. R^2 for this winter model was 45%, similar to [36]. The best-explained variability of $PM_{2.5}$ in the winter season was 90%, reported in [38], which used six independent predictor variables.

The initial step of the model development produced a list of predictors for the Novi Sad summer $PM_{2.5}$ LUR model (Table 6) that had only source predictors serving as proxies for traffic intensity. Target $PM_{2.5}$ seasonal concentration was inferred based on a measuring campaign that was conducted during the non-heating season months of July–September. These raw measurements were corrected to obtain seasonal averages using the ESCAPE procedure [52].

The iterative development procedure resulted in the seven models shown in Table 7. The procedure started with a univariate model with *SECONDARYROADLENGTH_1000m* as a predictor. This predictor was calculated over a large buffer area and varied with the number of secondary roads in the part of the city encircled by the buffer. The iterative procedure then continued and arrived at the bivariate model with *SECONDARY-*

ROADLENGTH_1000m and *ROADLENGTH_50m* (number of roads in a very small buffer around the site) as predictors. Note that so far, all models derived from the stepwise procedure have statistically significant predictors; however, also note that *VIF* is increasing. Finally, following the stepwise ESCAPE procedure, we arrived at the trivariate model with *SECONDARYROADLENGTH_1000m*, *ROADLENGTH_50m* and *ROADLENGTH_50_300* (number of roads in a circular ring with inner and outer diameters of 50 and 300 m, respectively) and explains a total of *adj.* R^2 = 0.570. Here, we stop the ESCAPE procedure since no new predictors can be added that increase *adj.* R^2. Note also that the *VIF* parameter is further increased, indicating a mild collinearity between the predictors. It is known that such collinearity between the predictors does not reduce the explained variance; however, it does reduce the statistical significance of the predictors. The ESCAPE procedure mitigates this by omitting, in the final step of the model development, predictors that are not statistically significant. For purposes of completeness, we have also, in Appendix B, added validation of the first two models in the stepwise procedure, since these were fully statistically significant but were not reached by direct application of the ESCAPE procedure.

In the summer seasonal model developed for the city of Novi Sad, *ROADLENGTH_50m* was the only significant predictor variable included in the model, with an explained variance of $PM_{2.5}$ concentration of 40%. The road length predictor within a buffer of 50 m had a higher value of R = 0.658 than in the winter. This can be explained by the fact that small-scale traffic variations are more easily observed due to fewer variations in emission sources of $PM_{2.5}$ in urban environments in the summer season. Few existing studies have efficiently used road length without linked traffic, but good road classification is needed for their application as potential predictor variables [70,71].

In comparison to our $PM_{2.5}$_LUR_{SUMMER} model and achieved percentage of explained variance, models in [32,37,38] explained 72%, 50% and 59% of $PM_{2.5}$ variance, respectively. In all three studies, predictor variable total lengths of local roads were included in the final LUR models. The summer model developed by Bertazzon et al. [37] included the sum of several road segment lengths in a buffer of 750 m as a final predictor. Contrary to previously mentioned models and our LUR_{SUMMER} model, the model developed by Jeffrey [72] used explanatory variables based on road classes and explained 97% of PM summer variability using additional predictor variables, including temperature, average air pressure, altitude, humidity and precipitation. The winter model's final predictors developed by [35] were the same as for their summer season model, which explained 52% of summer variability. The lowest explained $PM_{2.5}$ variability for summer among reviewed articles was 36% and the explanatory variables included in the final model were the length of railways in a 1000 m buffer, distance to the nearest open grills, population/building density, waste burning sites and distance to nearest refuse transfer station [75].

Both the winter and summer LUR models outperform the AOD satellite data-driven approach, as evidenced by the consistently lower RMSE values for the winter and summer datasets (see Appendices B and C). This suggests that incorporating LUR predictors enables better capturing of local-scale variations in $PM_{2.5}$ concentrations compared to AOD satellite-derived data. While satellite observations can offer broader coverage, their limited ability to resolve fine-scale variations results in higher RMSE values, highlighting the importance of integrating LUR-specific predictors for more accurate air quality assessments.

5. Conclusions

The developed $PM_{2.5}$_LUR_{WINTER} and $PM_{2.5}$_LUR_{SUMMER} models are seasonal land use regression models. These models represent an advancement in the field of land use regression (LUR) for $PM_{2.5}$ in the region.

The $PM_{2.5}$_LUR_{WINTER} model includes two predictors; the first one can be associated with individual heating sources in the city. Along with the *suburb_3000m* predictor as a proxy for combustion processes in individual heating sources, predictor *ROADLENGTH_50m* stood out as the predictor of traffic originating $PM_{2.5}$ in the winter model, quantifying the influence on $PM_{2.5}$ particulate matter emission during the winter due to close vicinity

roads. The $PM_{2.5}$_LUR_{SUMMER} model emphasizes the influence of traffic as the most important emission source in the summer, though only one predictor *ROADLENGTH_50m* was statistically significant following the final step of the ESCAPE procedure. The lack of street-level traffic data probably affected the achieved percentage of variability explained by both models and including currently unavailable street-level traffic model would be the straightforward path for improvement of the model.

The results obtained in this study could be of direct use in the assessment of air pollution-related health risks in the municipality and contribute scientifically and practically to local authorities dealing with air quality control. Since models showed good predictive accuracy, developed seasonal $PM_{2.5}$ LUR models for Novi Sad can be used in information products as base maps of fine particulate matter pollution.

As part of further research opportunities, we plan to refine developed models through additional measurement campaigns, utilizing low-cost sensor data and adding more exact traffic and heating predictors for emissions instead of proxies, thus increasing the interpretability of the model. Low-cost sensor data can be used to increase the spatial and temporal resolution of the seasonal models by fusing measurement data with modelled pollution data. Another possible direction of future research that may bring improvements to heating and non-heating season model predictive efficiency is the inclusion of machine learning algorithms and more complex models utilizing satellite data since a simple aerosol optical depth model gave promising results in this study.

Author Contributions: Conceptualization, S.D., M.J.-S. and M.D.; methodology, S.D., M.J.-S. and M.D.; validation S.D, M.Ž., Ž.Ć. and M.D.; investigation, S.D., Ž.Ć. and M.D.; resources, J.R., M.J.-S. and M.D.; data curation, S.D.; software, Ž.Ć. and M.D.; formal analysis S.D., M.Ž., Ž.Ć., M.J.-S. and M.D.; writing—original draft S.D.; writing—review and editing, S.D., J.R., M.Ž., M.J.-S. and M.D.; visualization, S.D. and M.D.; supervision, J.R. and M.D.; project administration, M.J.-S. and M.D.; funding acquisition, M.J.-S. and M.D. All authors have read and agreed to the published version of the manuscript.

Funding: This research was funded by the European Union's Horizon 2020 Research and Innovation Programme under the VIDIS project, grant number 952433. This research was also supported by the City Administration for Environmental Protection Novi Sad project no. VI-501-2/2022-35B-11, "Mapping particulate matter air pollution in near-real time in Novi Sad using data from sensor networks and statistical/physical modeling", the Ministry of Science, Technological Development and Innovation of the Republic of Serbia (contract numbers 451-03-66/2024-03/200017 and 451-03-65/2024-03/200156), the Faculty of Technical Sciences, University of Novi Sad through project "Scientific and Artistic Research Work of Researchers in Teaching and Associate Positions at the Faculty of Technical Sciences, University of Novi Sad" (No. 01-3394/1) and the Provincial Secretariat for Higher Education and Scientific Research, AP Vojvodina, Republic of Serbia (Grant number 142-451-3509/2023-01).

Institutional Review Board Statement: Not applicable.

Informed Consent Statement: Not applicable.

Data Availability Statement: Restrictions apply to the availability of some of the data used in this work. Data concerning traffic intensities are available from the corresponding author with the permission of the Public Company "Urbanism" in Novi Sad.

Acknowledgments: We are grateful to our colleague Maja Jovanovic for their contributions to the $PM_{2.5}$ measurement and validation, and for the fruitful discussions that improved this paper.

Conflicts of Interest: The authors declare no conflict of interest.

Appendix A

Potential predictor variables that were used during the development of the two seasonal (winter and summer) models were calculated as described in [76] and are included in Table A1. Predictors are split into the following categories: land cover, land use, local traffic density, road length, classes, distance from the river and population. Next to each

predictor, in the last column in Table A1, is the potential direction of effect. The direction of effect plays a role during model development and will be discussed further in the following section.

Table A1. List of potential predictor variables, units, buffer size and direction of effect of target variable $PM_{2.5}$.

Land Use/Land Cover Database	Database Name/Tag	Predictor Variable	Unit	Buffer Size	Direction of Effect
Corine land cover	Class1		m^2	300, 1000, 3000 m	+
	Class2				+
	Class3				-
	Class4				-
	Class5				-
Open street maps	landuse = building	building_area	m^2	300, 1000, 3000 m	+
	landuse = park	park_area			-
	landuse = industrial	industrial_area			+
	landuse = forest	forest_area			-
	landuse = farmland	suburban_area			+
	landuse = residential	resident_area			+
Local traffic density	A_class		number of vehicles per day^{-1} m	25, 50, 100, 200, 300, 500, 1000, 1500 m	+
	B_class				+
	C_class				+
Open street map (Road length and classes)	ROADLENGTH	ROADLENGTH	m	25, 50, 100, 200, 300, 500, 100, 1500 m	+
	PRIMARYROADLENGTH	PRIMARYROADLENGTH			+
	SECONDARYROADLENGTH	SECONDARYROADLENGTH			+
	TERTIARYROADLENGTH	TERTIARYROADLENGTH			+
	RESIDENTROADLENGTH	RESIDENTROADLENGTH			+
	DISTINVMAJOR1 and DISTINVMAJOR2	DISTINVMAJOR1 and DISTINVMAJOR2	m^{-1}, m^{-2}	Inverse distance and squared inverse distance	+
	DISTINVSECOND1 and DISTINVSECOND2	DISTINVSECOND1 and DISTINVSECOND2			+
	DISTINVTERT1 and DISTINVTERT2	DISTINVTERT1 and DISTINVTERT2			+
	DISTINVNEAR1 and DISTINVNEAR2	DISTINVNEAR1 and DISTINVNEAR2			+
Distance to the river	River Danube		m	NA	+
Population	Total population around measuring location, within a buffer		Number of inhabitants	300, 1000, 3000 m	+

Note. Class1—artificial area, Class2—agricultural areas, Class3—forest and semi natural areas, Class4—wetlands, Class5—water bodies, suburban_area—area of households, outside strictly urban areas, with household heating on solid fuels and private central heating, WIN_A—mean daily winter traffic densities for class A on all roads in a buffer (sum (traffic density × length of all road segments)), WIN_B—mean daily winter traffic densities for class B on all roads in a buffer (sum (traffic density × length of all road segments)), WIN_C—mean daily winter traffic densities for class C on all roads in a buffer (sum (traffic density × length of all road segments)), ROADLENGTH—length of all roads in a buffer, PRIMARYROADLENGTH—length of all primary roads in a buffer, SECONDARYROADLENGTH—length of all secondary roads in a buffer, TERTIARYROADLENGTH—length of all tertiary roads in a buffer, RESIDENTROADLENGTH—length of all resident roads in a buffer, DISTINVMAJOR1 and DISTINVMAJOR2—distance to the nearest primary road, DISTINVSECOND1 and DISTINVSECOND2—distance to the nearest secondary road, DISTINVTERT1 and DISTINVTERT2—distance to the nearest tertiary road, DISTINVNEAR1 and DISTINVNEAR2—distance to the nearest road. NA—Not applicable [53].

Different land cover classes, especially land use patterns, existing within the city have different impacts on urban air pollution and are strongly correlated with $PM_{2.5}$ concentration levels [77,78], along with traffic density, road length and road classes [79,80].

The selection of potential predictors must be in accordance with the specifics of the city and based on the main known emission sources and other factors that may influence $PM_{2.5}$ concentrations. The definitions of the majority of the predictors are equivalent to those in the ESCAPE study [24]. In this study, potential predictor directions of effect were kept the same for both seasons.

The land cover group of predictors, artificial surfaces and agricultural areas are given a positive direction of effect, while forests, wetlands and water areas have a negative direction. The agricultural area can be treated as a seasonal predictor, with a greater possible impact on $PM_{2.5}$ during the summer than the winter; however, in both seasons, certain agricultural activities such as straw burning are possible, resulting in a sharp increase in $PM_{2.5}$ concentration within a short time [77,78]. As a predictor, artificial surface can be divided into many subclasses; however, in this study, it was used collectively and treated as a contributor to $PM_{2.5}$ pollution due to its potential as a proxy for many primary and secondary anthropogenic emission sources and its stronger spatial association at small scales [81,82]. Besides the previously mentioned variables, every artificial surface, particularly larger ones, can cause urban heat islands, which can further transport air pollutants [82]. The predictors forest, wetland and water were assigned a negative direction of effect, based on the assumption of their potential to decrease $PM_{2.5}$ pollution. Green and (some) natural surfaces can be considered sinks for $PM_{2.5}$ due to the process of aerosol surface deposition [78]; however, vegetation capacity for deposition may change from season to season [81]. Proximity to water surfaces often provides better conditions for pollutant dispersion [78].

The group of land use predictors consists of buildings, parks and industrial, forest, suburban, and resident areas, of which only park and forest areas are associated with $PM_{2.5}$ concentration decrease, similar to forest, wetland, and water areas in the land cover predictors. Building areas can be treated as the main urban elements that affect $PM_{2.5}$ dispersion [79]. In the last few decades, Novi Sad has been in the phase of intensive urbanization characterized by changes in the urban structure of the city, with the construction of many new buildings, a mix of high-rise and low-rise buildings, and underground and above-ground garages. Considering that building areas are treated as a factor that increases PM pollution, especially because the populations of small areas with multi-story buildings create conditions for canyon street effects and possible increase in PM pollution. Industrial areas have similarities with artificial surfaces and generate a certain amount of $PM_{2.5}$ pollution. The residential area is also assigned a positive direction of effect and reflects the influence of urban life activities of inhabitants on $PM_{2.5}$ concentrations. The suburban area as defined in Table A1 is particularly used in this research as a proxy for the heating season's impact on $PM_{2.5}$ during winter and various characteristic activities of household areas such as agriculture and burning of certain biomass during the summer. Individual heating systems have a major influence on local air quality generally [83], as well as in Novi Sad, and with this predictor, we aimed to model pollution generated over a larger area, outside the local variations within the DH area. While "landuse = farmland" signifies rural areas, it can also be indirectly helpful for separating urban areas from suburbs. Since suburbs typically have lower population density compared to the city core and might have pockets of farmland on their fringes, the presence of "landuse = farmland" surrounding a designated urban area could indicate a suburban zone.

The predictor group local traffic density has a positive direction of effect on $PM_{2.5}$ pollution since 18 of the 21 measuring locations are traffic sites or sites that are near traffic. Direct traffic impacts include emissions from tailpipe exhausts, brake wear and tyre wear [84] as well as the impact of resuspended dust from roads [85].

Road length and classes as potential predictors consisting of the different road classes are used as a proxy for traffic density and are therefore assigned a positive direction of

effect. Road length as a proxy for traffic density has been used effectively in many scientific studies [86–88].

Appendix A.1. Land Cover, Land Use, Distance from the River and Population Density

Land cover data (Figure A1) in the form of vector and 100 m raster data were downloaded from the Corine Land Cover (CLC) website [89]. The data were categorized into five main CLC classes: artificial surfaces, agricultural areas, forest and seminatural land, wetlands and water bodies.

Land use data (Figure A2) were downloaded from the Open Street Map (OSM) website via a publicly available source [90]. Data were classified into building area, park area, industrial area, forest area, farm area and resident area.

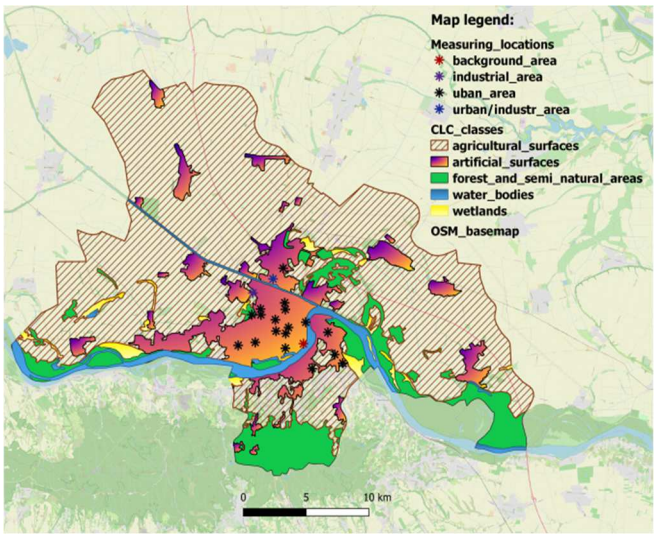

Figure A1. Corine Land Cover classes for Novi Sad, Petrovaradin and Sremska Kamenica and all settlements.

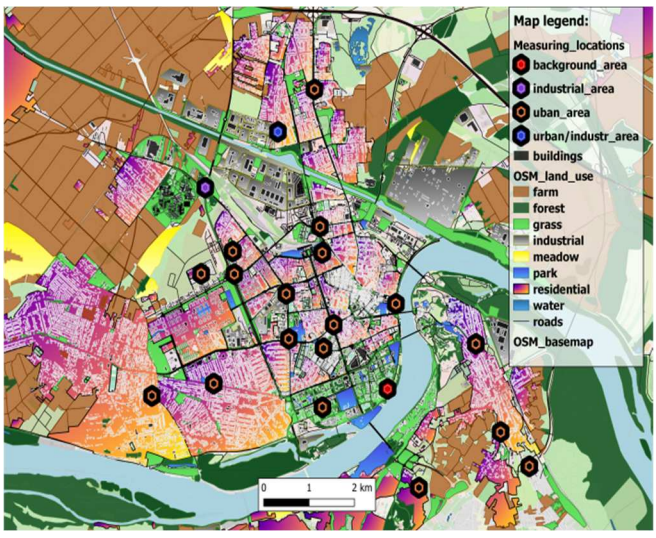

Figure A2. Open Street Map land use classes for Novi Sad, Petrovaradin and Sremska Kamenica.

Additional potential predictors are distance from the river and population density. Distance from the river is the aerial distance from each measuring site to the Danube River. Population data were collected from the public utility company "Informatika" in the form of the number of inhabitants per apartment in each street in the research area.

Appendix A.2. Local Traffic Intensity, Road Length and Classes

Traffic intensity data were collected from 31 automatic traffic counters (Figure A3) that are under the jurisdiction of the Institute for Urban Planning in Novi Sad. Vehicle count data were available at a resolution of 15 min. Traffic counters covered small parts of the streets, roundabouts and intersections. Vehicle counts were divided into classes A, B and C, where class A represents passenger cars and vans, class B represents different types of trucks and class C represents public transportation (city buses).

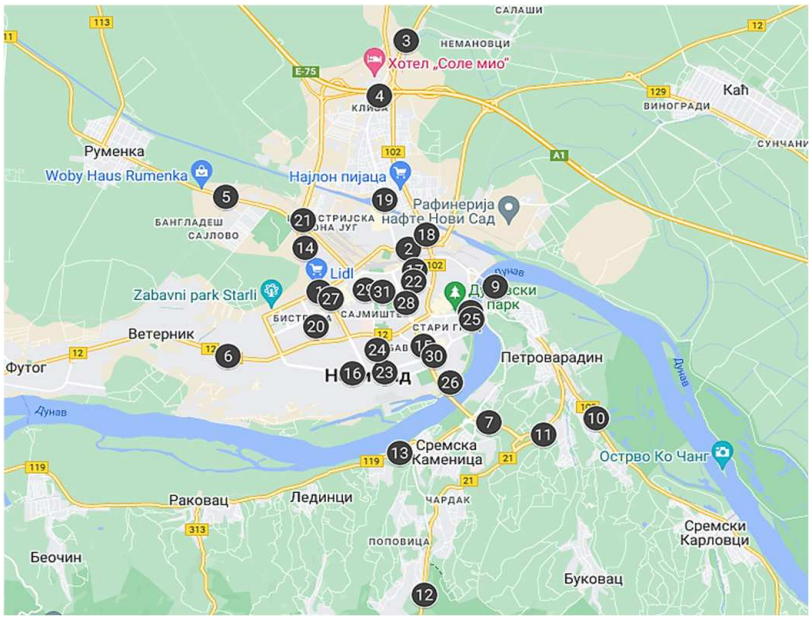

Figure A3. Traffic counter locations.

The traffic intensity predictor was not taken into account for the model development due to a lack of street-level traffic data for Novi Sad, and crude approximations of traffic intensity resulted in weak correlations with $PM_{2.5}$ in the heating and non-heating models.

Data on road classes in Novi Sad were collected from OSM (Figure A3) via [90] and were classified into primary, secondary, tertiary and residential road types. Based on OSM classification, primary, secondary, tertiary and residential roads are defined as:

- Primary—a major highway linking large towns
- Secondary—a highway that is not part of a major route but forms a link in the national route network (often links towns)
- Tertiary—roads connecting smaller settlements, or a road within large settlements that connect local centres (often links smaller towns and villages)
- Residential—roads that serve as access to housing, without the function of connecting settlements

Appendix B

The validation results of the final $PM_{2.5}$_LUR_{WINTER} model, generated using the LOOCV method, are presented in Table A2. The value of *adj.* R^2 ranges from 34 to 61% on the training set. The RMSE ranged from 3.79 to 4.11 for the training set, and for the left-out observation ($\mathbf{y}_{true}$), RMSE and MAE were 4.04 and 4.80 $\mu g/m^3$, respectively. The RMSE for the left-out observation falls within the RMSE range for the training set. Based on the obtained results, the tested winter model was stable and was not sensitive to excluded observations.

The results of the $PM_{2.5}$_LUR_{SUMMER} model validation, in which the only predictor was ROADLENGTH_50m, generated using the LOOCV method, are presented in Table A3. The value of *adj.* R^2 ranges from 31 to 45% for the training set. The *RMSE* coefficient ranges

from 2.74 to 3.01 for the training set, and on left-out observation (y_{true}), the RMSE and *MAE* are 2.80 and 3.17 $\mu g/m^3$, respectively. Note how the *RMSE* for the left-out observation falls within the *RMSE* range for the training set. Based on the obtained results, the tested winter model is stable and is not sensitive to excluded observations.

Table A2. Validation results of the final $PM_{2.5}$_LUR_{WINTER} model. Units for the *RMSE*, *MAE*, $y_{predicted}$, y_{true}, and Δy values are in $\mu g/m^3$.

Model		**$PM_{2.5}$_LUR_{WINTER}**								
Excluded Observation		***R^2***	***adj. R^2***	***F*-Statistic**	***p* Value**	***RMSE***	***MAE***	$y_{predicted}$	y_{true}	Δy
1	URB	0.618	0.573	13.76	0.000	3.82	3.20	32.44	25.57	6.87
2	URB	0.413	0.344	5.98	0.011	3.94	3.28	43.53	50.21	−6.68
3	URB/IND	0.570	0.520	11.28	0.001	3.92	3.32	37.76	43.77	−6.01
4	URB	0.63	0.586	14.46	0.000	3.86	3.27	31.69	38.19	−6.5
5	URB	0.594	0.547	12.45	0.000	4.10	3.50	33.02	34.17	−1.15
6	URB	0.654	0.613	16.08	0.000	3.79	3.22	25.13	32.89	−7.76
7	IND	0.621	0.577	13.94	0.000	3.86	3.06	47.45	39.65	7.8
8	URB	0.594	0.546	12.43	0.000	4.10	3.51	34.33	33.55	0.78
9	URB	0.618	0.573	13.75	0.000	3.81	3.14	32.61	25.25	7.36
10	URB	0.595	0.548	12.50	0.000	4.08	3.43	33.52	35.64	−2.12
11	URB	0.596	0.548	12.54	0.000	3.93	3.33	31.15	25.45	5.7
12	URB	0.589	0.541	12.20	0.001	4.09	3.49	35.22	36.81	−1.59
13	URB	0.601	0.554	12.78	0.000	4.07	3.46	37.41	34.16	3.25
14	URB	0.589	0.541	12.20	0.001	4.05	3.36	31.13	27.92	3.21
15	URB	0.616	0.571	13.66	0.000	3.97	3.25	30.66	35.63	−4.97
16	URB	0.581	0.532	11.79	0.001	4.10	3.51	29.23	28.37	0.86
17	BCG	0.609	0.564	13.26	0.000	3.93	3.29	32.84	27.39	5.45
18	URB	0.594	0.546	12.42	0.000	4.10	3.51	31.54	32.5	−0.96
19	URB	0.610	0.564	13.30	0.000	4.00	3.30	31.76	36.12	−4.36
20	URB	0.589	0.541	12.18	0.001	4.10	3.49	31.14	30	1.14
21	URB	0.565	0.514	11.06	0.001	4.11	3.53	25.92	26.2	−0.28

Note. R^2—coefficient of determination, *adj.* R^2—adjusted R^2, *p*-value—probability of *F*-statistic, *RMSE*—root mean square error of the model, *MAE*—mean absolute error of the model, $y_{predicted}$—model prediction at the left-out location, y_{true}—measurement at the left-out location, $\Delta y = y_{predicted} - y_{true}$ error of the prediction.

Table A3. Validation results of the final $PM_{2.5}$_LUR_{SUMMER} model. Units for the *RMSE*, *MAE*, $y_{predicted}$, y_{true}, and Δy values are in $\mu g/m^3$.

Model		**$PM_{2.5}$_LUR_{SUMMER}**								
Excluded Observation		***R^2***	***adj. R^2***	***F*-Statistic**	***p*-Value**	***RMSE***	***MAE***	$y_{predicted}$	y_{true}	Δy
1	URB	0.474	0.445	16.23	0.001	2.82	2.40	14.84	19.56	−4.72
2	URB	0.348	0.312	9.62	0.006	2.98	2.59	20.48	22.31	−1.83
3	URB/IND	0.433	0.401	13.73	0.002	2.99	2.64	15.43	14.22	1.21
4	URB	0.430	0.398	13.56	0.002	2.89	2.55	14.63	10.85	3.78
5	URB	0.427	0.395	13.42	0.002	2.88	2.55	14.47	10.49	3.98
6	URB	0.393	0.359	11.63	0.003	2.98	2.62	12.69	10.71	1.98
7	IND	0.429	0.398	13.54	0.002	3.01	2.68	17.35	17.14	0.21
8	URB	0.443	0.412	14.32	0.001	2.96	2.59	16.17	13.72	2.45
9	URB	0.408	0.375	12.42	0.002	3.00	2.68	12.47	12.19	0.28
10	URB	0.418	0.385	12.91	0.002	2.94	2.51	17.38	20.36	−2.98
11	URB	0.445	0.415	14.45	0.001	2.74	2.36	16.79	22.48	−5.69
12	URB	0.426	0.394	13.35	0.002	3.00	2.67	14.29	13.73	0.56
13	URB	0.394	0.360	11.70	0.003	2.98	2.59	22.65	20.62	2.03

Table A3. *Cont.*

Model		$PM_{2.5}_LUR_{SUMMER}$								
Excluded Observation		R^2	*adj.* R^2	*F*-Statistic	*p*-Value	*RMSE*	*MAE*	$y_{predicted}$	y_{true}	Δy
14	URB	0.462	0.432	15.46	0.001	2.93	2.49	12.93	16.15	−3.22
15	URB	0.467	0.438	15.78	0.001	2.90	2.54	18.01	14.41	3.6
16	URB	0.439	0.408	14.09	0.001	2.97	2.55	15.63	17.82	−2.19
17	BCG	0.475	0.445	16.26	0.001	2.83	2.51	16.84	12.22	4.62
18	URB	0.482	0.453	16.76	0.001	2.87	2.43	11.89	16.15	−4.26
19	URB	0.451	0.420	14.76	0.001	2.95	2.58	17.38	14.81	2.57
20	URB	0.453	0.422	14.90	0.001	2.85	2.42	15.92	20.32	−4.4
21	URB	0.391	0.357	11.54	0.003	2.97	2.61	12.72	10.47	2.25

Note. R^2—coefficient of determination, *adj.* R^2—adjusted R^2, *p*-value—probability of *F*-statistic, *RMSE*—root mean square error, *MAE*—mean absolute error of the model, $y_{predicted}$—model prediction at the left-out location, y_{true}—measurement at the left-out location, $\Delta y = y_{predicted} - y_{true}$ error of the prediction.

Table A4. Validation results of the first LUR summer model 1 (with predictor SECONDARY-ROADLENGTH_1000m). Units for the *RMSE*, *MAE*, $y_{predicted}$, y_{true}, and Δy values are in $\mu g/m^3$.

Model		$PM_{2.5}_LUR_{SUMMER}$ (Model 1)								
Excluded Observation		R^2	*adj.* R^2	*F*-Statistic	*p* Value	*RMSE*	*MAE*	$y_{predicted}$	y_{true}	Δy
1	URB	0.472	0.443	16.10	0.001	2.83	2.22	16.16	19.56	−3.40
2	URB	0.490	0.462	17.29	0.001	2.64	2.11	16.52	22.31	−5.79
3	URB/IND	0.460	0.43	15.33	0.001	2.92	2.36	14.83	14.22	0.61
4	URB	0.418	0.385	12.92	0.002	2.92	2.37	11.45	10.85	0.60
5	URB	0.420	0.387	13.01	0.002	2.90	2.33	12.37	10.49	1.88
6	URB	0.589	0.567	25.85	0.000	2.45	2.02	18.14	10.71	7.43
7	IND	0.461	0.431	15.37	0.001	2.92	2.35	17.77	17.14	0.63
8	URB	0.465	0.435	15.64	0.001	2.90	2.27	11.88	13.72	−1.84
9	URB	0.443	0.412	14.32	0.001	2.91	2.35	13.29	12.19	1.10
10	URB	0.449	0.418	14.67	0.001	2.86	2.26	17.45	20.36	−2.91
11	URB	0.382	0.348	11.14	0.004	2.89	2.32	20.30	22.48	−2.18
12	URB	0.462	0.433	15.48	0.001	2.91	2.29	12.16	13.73	−1.57
13	URB	0.423	0.391	13.21	0.002	2.91	2.33	19.20	20.62	−1.42
14	URB	0.467	0.438	15.79	0.001	2.91	2.32	17.41	16.15	1.26
15	URB	0.489	0.461	17.23	0.001	2.84	2.23	17.56	14.41	3.15
16	URB	0.455	0.425	15.05	0.001	2.92	2.38	17.66	17.82	−0.16
17	BCG	0.458	0.428	15.21	0.001	2.88	2.29	14.64	12.22	2.42
18	URB	0.529	0.502	20.19	0.000	2.74	2.09	11.19	16.15	−4.96
19	URB	0.471	0.441	16.01	0.001	2.90	2.30	16.59	14.81	1.78
20	URB	0.441	0.41	14.22	0.001	2.88	2.28	17.90	20.32	−2.42
21	URB	0.487	0.458	17.08	0.001	2.72	2.17	15.36	10.47	4.89

Note. R^2—coefficient of determination, *adj.* R^2—adjusted R^2, *p*-value—probability of *F*-statistic, *RMSE*—root mean square error, *MAE*—mean absolute error of the model, $y_{predicted}$—model prediction at the left-out location, y_{true}—measurement at the left-out location, $\Delta y = y_{predicted} - y_{true}$ error of the prediction.

Table A5. Validation results of the second LUR summer model 2 (with predictors *SECONDARY-ROADLENGTH_1000m* and *ROADLENGTH_50m*). Units for the *RMSE*, *MAE*, $y_{predicted}$, y_{true}, and Δy values are in $\mu g/m^3$.

Model		$PM_{2.5}_LUR_{SUMMER}$ (Model 2)								
Excluded Observation		R^2	*adj.* R^2	*F*-Statistic	*p*-Value	*RMSE*	*MAE*	$y_{predicted}$	y_{true}	Δy
1	URB	0.619	0.574	13.8	0.000	2.40	2.04	15.48	19.56	−4.08
2	URB	0.552	0.500	10.48	0.001	2.47	2.02	18.82	22.31	−3.49

Table A5. *Cont.*

Model		$PM_{2.5}$_LUR_{SUMMER} (Model 2)								
Excluded Observation		R^2	*adj.* R^2	*F*-Statistic	*p*-Value	*RMSE*	*MAE*	$y_{predicted}$	y_{true}	Δy
3	URB/IND	0.586	0.537	12.03	0.001	2.56	2.19	14.90	14.22	0.68
4	URB	0.557	0.505	10.69	0.001	2.55	2.16	12.14	10.85	1.29
5	URB	0.560	0.508	10.8	0.001	2.52	2.13	12.60	10.49	2.11
6	URB	0.631	0.588	14.56	0.000	2.32	1.91	16.35	10.71	5.64
7	IND	0.588	0.540	12.14	0.001	2.55	2.17	18.17	17.14	1.03
8	URB	0.582	0.533	11.85	0.001	2.56	2.21	13.43	13.72	−0.29
9	URB	0.570	0.520	11.27	0.001	2.56	2.21	11.88	12.19	−0.31
10	URB	0.574	0.523	11.44	0.001	2.51	2.11	18.02	20.36	−2.34
11	URB	0.544	0.490	10.14	0.001	2.49	2.10	19.30	22.48	−3.18
12	URB	0.588	0.539	12.11	0.001	2.55	2.15	12.32	13.73	−1.41
13	URB	0.565	0.514	11.03	0.001	2.53	2.12	22.92	20.62	2.30
14	URB	0.591	0.543	12.27	0.001	2.55	2.18	15.04	16.15	−1.11
15	URB	0.632	0.589	14.60	0.000	2.41	2.02	18.41	14.41	4.00
16	URB	0.584	0.535	11.93	0.001	2.56	2.19	16.98	17.82	−0.84
17	BCG	0.607	0.561	13.12	0.000	2.45	2.07	15.71	12.22	3.49
18	URB	0.685	0.648	18.52	0.000	2.24	1.94	10.04	16.15	−6.11
19	URB	0.605	0.559	13.05	0.000	2.50	2.10	17.35	14.81	2.54
20	URB	0.585	0.536	11.98	0.001	2.48	2.09	17.32	20.32	−3.00
21	URB	0.576	0.527	11.57	0.001	2.47	2.04	13.67	10.47	3.20

Note. R^2—coefficient of determination, *adj.* R^2—adjusted R^2, *p*-value—probability of *F*-statistic, *RMSE*—root mean square error, *MAE*—mean absolute error of the model, $y_{predicted}$—model prediction at the left-out location, y_{true}—measurement at the left-out location, $\Delta y = y_{predicted} - y_{true}$ error of the prediction.

Appendix C

The validation results for the $PM_{2.5}AOD_{WINTER}$ and $PM_{2.5}AOD_{SUMMER}$ models are presented in Table A6. The obtained RMSE values ranged from 5.25 to 6.80 μg/m^3 for winter and from 3.44 to 3.83 for summer. Based on the obtained results, both the winter and summer models are stable and are not sensitive to excluded observations.

Table A6. Validation results of the $PM_{2.5}$_AOD_{WINTER} and $PM_{2.5}$_AOD_{SUMMER} models. All units in the table are in μg/m^3.

Model		$PM_{2.5}$_AOD_{WINTER}					$PM_{2.5}$_AOD_{SUMMER}				
Excluded Observation		*RMSE*	*MAE*	$y_{predicted}$	y_{true}	Δy	*RMSE*	*MAE*	$y_{predicted}$	y_{true}	Δy
1	URB	6.56	5.03	33.87	25.57	8.30	3.72	3.12	15.26	19.56	−4.3
2	URB	5.25	4.73	30.45	50.21	−19.76	3.44	2.94	14.59	22.31	−7.72
3	URB/IND	6.50	5.16	34.56	43.77	−9.21	3.82	3.3	15.63	14.22	1.41
4	URB	6.74	5.35	33.95	38.19	−4.24	3.71	3.17	15.31	10.85	4.46
5	URB	6.80	5.50	33.83	34.17	−0.34	3.64	3.12	16.03	10.49	5.54
6	URB	6.80	5.50	32.69	32.89	−0.20	3.72	3.18	14.94	10.71	4.23
7	IND	6.60	5.22	32.16	39.65	−7.49	3.81	3.26	15.32	17.14	−1.82
8	URB	6.78	5.42	31.14	33.55	−2.41	3.78	3.24	16.59	13.72	2.87
9	URB	6.64	5.12	31.95	25.25	6.70	3.77	3.22	15.43	12.19	3.24
10	URB	6.77	5.40	32.70	35.64	−2.94	3.79	3.21	17.77	20.36	−2.59
11	URB	6.51	4.99	34.55	25.45	9.10	3.53	2.99	15.58	22.48	−6.9
12	URB	6.79	5.43	34.72	36.81	−2.09	3.81	3.28	15.68	13.73	1.95
13	URB	6.79	5.42	31.91	34.16	−2.25	3.69	3.1	15.86	20.62	−4.76

Table A6. *Cont.*

Model		$PM_{2.5}$_AOD_{WINTER}					$PM_{2.5}$_AOD_{SUMMER}				
Excluded Observation		*RMSE*	*MAE*	$y_{predicted}$	y_{true}	Δy	*RMSE*	*MAE*	$y_{predicted}$	y_{true}	Δy
14	URB	6.66	5.14	34.23	27.92	6.31	3.82	3.29	14.79	16.15	−1.36
15	URB	6.72	5.32	30.88	35.63	−4.75	3.83	3.34	15.04	14.41	0.63
16	URB	6.68	5.16	34.19	28.37	5.82	3.77	3.18	14.54	17.82	−3.28
17	BCG	6.64	5.11	34.26	27.39	6.87	3.79	3.24	14.96	12.22	2.74
18	URB	6.80	5.49	32.06	32.50	−0.44	3.83	3.35	16.35	16.15	0.2
19	URB	6.78	5.41	33.42	36.12	−2.70	3.82	3.3	16.34	14.81	1.53
20	URB	6.67	5.15	36.08	30.00	6.08	3.8	3.22	17.84	20.32	−2.48
21	URB	6.59	5.06	33.96	26.20	7.76	3.56	3.08	17.05	10.47	6.58

Note: *RMSE*—root mean square error, *MAE*—mean absolute error of the model. $y_{predicted}$—model prediction at the left-out location, y_{true}—measurement at the left-out location, $\Delta y = y_{predicted} - y_{true}$ error of the prediction.

Appendix D

Seasonal $PM_{2.5}$ concentrations showed strong spatial variations, particularly during the winter (see Table 3, variance). Seasonal $PM_{2.5}$ concentrations were also higher during the winter season, ranging from 25.25 to 50.21 μg/m^3, as shown in Table 2.

During the winter season, higher concentrations, with ranges 33.53–67.48 μg/m^3, 26.39–62.67 μg/m^3, 5.89–62.39 μg/m^3, 24.41–55.30 μg/m^3, 21.71–46.36 μg/m^3 and 27.43–43.06 μg/m^3, were measured at sites 2 (URB), 7 (IND), 8 (URB), 3 (URB) and 4 (URB) in the IH area and site 19 (URB), on the border of DH and the IH area, respectively (Figure 2b). All sites had the same property of traffic presence on primary and secondary roads, consisting of class A, B and C vehicles, except URB sites (sites 3 and 4), which were in residential areas with central heating or using wood or solid fossil fuels. The rest of the measured concentrations in the IH area ranged from 28.97 to 39.04 μg/m^3 at sites 12 (URB), 10 (URB), 15(URB), 5 (URB) and 18 (URB). Sites 12, 10 and 15 had the same traffic property, with traffic present on primary and secondary road types, consisting of class A, B, and C vehicles, while sites 5 and 18 are in domestic residential areas. Within the DH area sites, the concentration at sites 1 (URB, had the lowest minimum and highest maximum concentrations), 13 (URB), 6 (URB), 20 (URB, near the river), 14 (URB) and 11 (URB) ranged from 7.85 to 38.07 μg/m^3. Of all sites in the vicinity of traffic, to various extents, only site 6 is within a strictly residential area, with DH nearby, and site 13, with higher traffic intensity compared to the other sites, consisting mostly of class A and C vehicles. The rest of the measured concentration levels at sites 17 (BCG, near the river), 21 (URB), 16 (URB) and 9 (URB) in the DH area ranged from 21.63 to 31.96 μg/m^3. Site 17 is near the local BCG measuring station, so it was treated as a BCG site as well; however, concentrations at this site were not the lowest compared to the other sites' concentrations. Sites 21 and 9 were in the residential URB area, with low residential traffic intensities, while site 16 was in the vicinity of the intersection, with traffic consisting of class A and C vehicles. Higher concentrations of PM during the winter were also reported following seasonal PM research conducted by [91], emphasizing the impact of coal combustion processes for heating, and the absence of vegetation and its reduced adsorption capacity of $PM_{2.5}$ in winter.

Summer $PM_{2.5}$ concentrations ranged from 10.47 to 22.48 μg/m^3, as shown in Table 2. In the summer period, the highest concentrations measured over 48 h—in the range of 12.76–54.33 μg/m^3—were measured at site 11 (URB), although there was a construction site in the vicinity during the campaign. Concentration ranges of 11.98–30.62 μg/m^3 were measured at sites 13 (urban, high traffic), 2 (URB), 7 (IND, high traffic), 20 (URB), 10 (URB) and 1 (URB). All these sites are in close proximity to lower, moderate or higher traffic-intensity areas. Lower concentrations measured over 48 h ranged from 10.48 to 19.27 μg/m^3 were measured at sites 18 (URB), 14 (URB), 16 (URB), 8 (URB), 3 (URB/IND), 19 (URB), 12 (URB), 15 (URB), 17 (BCG) and 9 (URB), with the lowest traffic intensities at site 18 and no traffic on site 17. At sites 4 (URB), 6 (URB), 5 (URB) and 21 (URB), which had very low traffic intensities, the lowest $PM_{2.5}$ concentrations were in the range 6.77–12.48 μg/m^3.

References

1. European Environment Agency. *The European Environment—State and Outlook 2015: Synthesis Report*; European Environment Agency: Copenhagen, Denmark, 2015; ISBN 978-92-9213-515-7.
2. Wang, J.; Ogawa, S. Effects of Meteorological Conditions on $PM_{2.5}$ Concentrations in Nagasaki, Japan. *Int. J. Environ. Res. Public Health* **2015**, *12*, 9089–9101. [CrossRef]
3. World Health Organization. *Health Effects of Particulate Matter: Policy Implications for Countries in Eastern Europe, Caucasus and Central Asia*; World Health Organization, Regional Office for Europe: Copenhagen, Denmark, 2013; pp. 115–137.
4. Huang, L.; Zhang, C.; Bi, J. Development of Land Use Regression Models for $PM_{2.5}$, SO_2, NO_2 and O_3 in Nanjing, China. *Environ. Res.* **2017**, *158*, 542–552. [CrossRef] [PubMed]
5. Üzmez, Ö.Ö. Atmospheric concentrations of inorganic pollutants (NO_2, SO_2 and ozone) in Eskişehir: Spatial and vertical variations, weekday-weekend differences. *Anadolu Univ. J. Sci. Technol. A—Appl. Sci. Eng.* **2018**, *19*, 523–535. [CrossRef]
6. Bravo, M.A.; Fuentes, M.; Zhang, Y.; Burr, M.J.; Bell, M.L. Comparison of Exposure Estimation Methods for Air Pollutants: Ambient Monitoring Data and Regional Air Quality Simulation. *Environ. Res.* **2012**, *116*, 1–10. [CrossRef] [PubMed]
7. den Bossche, J.V.; de Baets, B.; Verwaeren, J.; Botteldooren, D.; Theunis, J. Development and Evaluation of Land Use Regression Models for Black Carbon Based on Bicycle and Pedestrian Measurements in the Urban Environment. *Environ. Model. Softw.* **2018**, *99*, 58–69. [CrossRef]
8. Larkin, A.; Anenberg, S.; Goldberg, D.L.; Mohegh, A.; Brauer, M.; Hystad, P. A Global Spatial-Temporal Land Use Regression Model for Nitrogen Dioxide Air Pollution. *Front. Environ. Sci.* **2023**, *11*, 1125979. [CrossRef]
9. Jin, L.; Berman, J.D.; Warren, J.L.; Levy, J.I.; Thurston, G.; Zhang, Y.; Xu, X.; Wang, S.; Zhang, Y.; Bell, M.L. A Land Use Regression Model of Nitrogen Dioxide and Fine Particulate Matter in a Complex Urban Core in Lanzhou, China. *Environ. Res.* **2019**, *177*, 108597. [CrossRef]
10. Cong-Thanh, T.; Tuyen, N.N.; Hang, N.T.T. Development of Environmental Data for Land Use Regression Models to Assess Fine Particulate Matter Pollution in Ho Chi Minh City. *IOP Conf. Ser. Earth Environ. Sci.* **2023**, *1170*, 012020. [CrossRef]
11. Mo, Y.; Booker, D.; Zhao, S.; Tang, J.; Jiang, H.; Shen, J.; Chen, D.; Li, J.; Jones, K.C.; Zhang, G. The Application of Land Use Regression Model to Investigate Spatiotemporal Variations of $PM_{2.5}$ in Guangzhou, China: Implications for the Public Health Benefits of $PM_{2.5}$ Reduction. *Sci. Total Environ.* **2021**, *778*, 146305. [CrossRef]
12. Morley, D.W.; Gulliver, J. A Land Use Regression Variable Generation, Modelling and Prediction Tool for Air Pollution Exposure Assessment. *Environ. Model. Softw.* **2018**, *105*, 17–23. [CrossRef]
13. Qi, M.; Dixit, K.; Marshall, J.D.; Zhang, W.; Hankey, S. National Land Use Regression Model for NO_2 Using Street View Imagery and Satellite Observations. *Environ. Sci. Technol.* **2022**, *56*, 13499–13509. [CrossRef] [PubMed]
14. Eeftens, M.; Beelen, R.; De Hoogh, K.; Bellander, T.; Cesaroni, G.; Cirach, M.; Declercq, C.; Dedele, A.; Dons, E.; De Nazelle, A.; et al. Development of Land Use Regression Models for $PM_{2.5}$, $PM_{2.5}$ Absorbance, PM_{10} and PM coarse in 20 European Study Areas; Results of the ESCAPE Project. *Environ. Sci. Technol.* **2012**, *46*, 11195–11205. [CrossRef] [PubMed]
15. Das, K.; Das Chatterjee, N.; Jana, D.; Bhattacharya, R.K. Application of Land-Use Regression Model with Regularization Algorithm to Assess $PM_{2.5}$ and PM_{10} Concentration and Health Risk in Kolkata Metropolitan. *Urban Clim.* **2023**, *49*, 101473. [CrossRef]
16. Ge, Y.; Fu, Q.; Yi, M.; Chao, Y.; Lei, X.; Xu, X.; Yang, Z.; Hu, J.; Kan, H.; Cai, J. High Spatial Resolution Land-Use Regression Model for Urban Ultrafine Particle Exposure Assessment in Shanghai, China. *Sci. Total Environ.* **2022**, *816*, 151633. [CrossRef]
17. Enkhjargal, O.; Lamchin, M.; Chambers, J.; You, X.Y. Linear and Nonlinear Land Use Regression Approach for Modelling $PM_{2.5}$ Concentration in Ulaanbaatar, Mongolia during Peak Hours. *Remote Sens.* **2023**, *15*, 1174. [CrossRef]
18. Karimi, B.; Shokrinezhad, B. Spatial Variation of Ambient $PM_{2.5}$ and PM_{10} in the Industrial City of Arak, Iran: A Land-Use Regression. *Atmos. Pollut. Res.* **2021**, *12*, 101235. [CrossRef]
19. Luminati, O.; Ledebur de Antas de Campos, B.; Flückiger, B.; Brentani, A.; Röösli, M.; Fink, G.; de Hoogh, K. Land Use Regression Modelling of NO_2 in São Paulo, Brazil. *Environ. Pollut.* **2021**, *289*, 117832. [CrossRef]
20. Chen, L.; Gao, S.; Zhang, H.; Sun, Y.; Ma, Z.; Vedal, S.; Mao, J.; Bai, Z. Spatiotemporal Modeling of $PM_{2.5}$ Concentrations at the National Scale Combining Land Use Regression and Bayesian Maximum Entropy in China. *Environ. Int.* **2018**, *116*, 300–307. [CrossRef]
21. Xu, H.; Bechle, M.J.; Wang, M.; Szpiro, A.A.; Vedal, S.; Bai, Y.; Marshall, J.D. National $PM_{2.5}$ and NO_2 Exposure Models for China Based on Land Use Regression, Satellite Measurements, and Universal Kriging. *Sci. Total Environ.* **2019**, *655*, 423–433. [CrossRef]
22. Zhou, T.; Fang, S.; Jin, L.; Li, X.; Song, X.; Wang, Y.; Zhou, X.; Bai, Y.; Ma, X. Development of Land Use Regression Models to Characterise Spatial Patterns of Particulate Matter and Ozone in Urban Areas of Lanzhou. *Urban Clim.* **2024**, *55*, 101879. [CrossRef]
23. Azmi, W.N.F.W.; Pillai, T.R.; Latif, M.T.; Koshy, S.; Shaharudin, R. Application of Land Use Regression Model to Assess Outdoor Air Pollution Exposure: A Review. *Environ. Adv.* **2023**, *11*, 100353. [CrossRef]
24. Wang, M.; Beelen, R.; Bellander, T.; Birk, M.; Cesaroni, G.; Cirach, M.; Cyrys, J.; de Hoogh, K.; Declercq, C.; Dimakopoulou, K. Performance of Multi-City Land Use Regression Models for Nitrogen Dioxide and Fine Particles. *Environ. Health Perspect.* **2014**, *122*, 843–849. [CrossRef]
25. Ma, X.; Zou, B.; Deng, J.; Gao, J.; Longley, I.; Xiao, S.; Guo, B.; Wu, Y.; Xu, T.; Xu, X.; et al. A Comprehensive Review of the Development of Land Use Regression Approaches for Modeling Spatiotemporal Variations of Ambient Air Pollution: A Perspective from 2011 to 2023. *Environ. Int.* **2024**, *183*, 108430. [CrossRef] [PubMed]

26. Harper, A.; Baker, P.N.; Xia, Y.; Kuang, T.; Zhang, H.; Chen, Y.; Han, T.L.; Gulliver, J. Development of Spatiotemporal Land Use Regression Models for $PM_{2.5}$ and NO_2 in Chongqing, China, and Exposure Assessment for the CLIMB Study. *Atmos. Pollut. Res.* **2021**, *12*, 101096. [CrossRef]
27. Hsu, C.Y.; Hsu, W.T.; Mou, C.Y.; Wong, P.Y.; Da Wu, C.; Chen, Y.C. Exposure Estimates of $PM_{2.5}$ Using the Land-Use Regression with Machine Learning and Microenvironmental Exposure Models for Elders: Validation and Comparison. *Atmos. Environ.* **2024**, *318*, 120209. [CrossRef]
28. Li, Z.; Ho, K.F.; Chuang, H.C.; Yim, S.H.L. Development and Intercity Transferability of Land-Use Regression Models for Predicting Ambient PM_{10}, $PM_{2.5}$, NO_2 and O_3 Concentrations in Northern Taiwan. *Atmos. Chem. Phys.* **2021**, *21*, 5063–5078. [CrossRef]
29. Wong, P.Y.; Lee, H.Y.; Zeng, Y.T.; Chern, Y.R.; Chen, N.T.; Lung, S.C.C.; Su, H.J.; Wu, C.D. Using a Land Use Regression Model with Machine Learning to Estimate Ground Level $PM_{2.5}$. *Environ. Pollut.* **2021**, *277*, 116846. [CrossRef] [PubMed]
30. Zeng, L.; Hang, J.; Wang, X.; Shao, M. Influence of Urban Spatial and Socioeconomic Parameters on $PM_{2.5}$ at Subdistrict Level: A Land Use Regression Study in Shenzhen, China. *J. Environ. Sci.* **2022**, *114*, 485–502. [CrossRef] [PubMed]
31. Zhang, Y.; Li, Z.; Bai, K.; Wei, Y.; Xie, Y.; Zhang, Y.; Ou, Y.; Cohen, J.; Zhang, Y.; Peng, Z.; et al. Satellite Remote Sensing of Atmospheric Particulate Matter Mass Concentration: Advances, Challenges, and Perspectives. *Fundam. Res.* **2021**, *1*, 240–258. [CrossRef]
32. Zheng, S.; Zhang, C.; Wu, X. Estimating $PM_{2.5}$ Concentrations Using an Improved Land Use Regression Model in Zhejiang, China. *Atmosphere* **2022**, *13*, 1273. [CrossRef]
33. Bo, M.; Salizzoni, P.; Clerico, M.; Buccolieri, R. Assessment of Indoor-Outdoor Particulate Matter Air Pollution: A Review. *Atmosphere* **2017**, *8*, 136. [CrossRef]
34. Rodriguez-Villamizar, L.A.; Rojas, Y.; Herrera, V.; Jiménez, J.G.P.; Rojas-Sánchez, O.A.; Villegas, J.O.; Rojas, O.M.; Salas, W.; Orrego, A.Z.; Castillo, M.; et al. Intra-Urban Variability of Long-Term Exposure to $PM_{2.5}$ and NO_2 in five Cities in Colombia. *Environ. Sci. Pollut. Res. Int.* **2024**, *31*, 3207–3221. [CrossRef] [PubMed]
35. Shi, T.; Hu, Y.; Liu, M.; Li, C.; Zhang, C.; Liu, C. Land Use Regression Modelling of $PM_{2.5}$ Spatial Variations in Different Seasons in Urban Areas. *Sci. Total Environ.* **2020**, *743*, 140744. [CrossRef] [PubMed]
36. Wu, J.; Li, J.; Peng, J.; Li, W.; Xu, G.; Dong, C. Applying Land Use Regression Model to Estimate Spatial Variation of $PM_{2.5}$ in Beijing, China. *Environ. Sci. Pollut. Res. Int.* **2015**, *22*, 7045–7061. [CrossRef] [PubMed]
37. Bertazzon, S.; Underwood, F.; Johnson, M.; Zhang, J. Land Use Regression of Particulate Matter in Calgary, Canada. In Proceedings of the International Conference on GIScience Short Paper Proceedings, Montreal, QC, Canada, 27–30 September 2016; Volume 1, pp. 17–20. [CrossRef]
38. Miri, M.; Ghassoun, Y.; Dovlatabadi, A.; Ebrahimnejad, A.; Löwner, M.O. Estimate Annual and Seasonal PM_1, $PM_{2.5}$ and PM_{10} Concentrations Using Land Use Regression Model. *Ecotoxicol. Environ. Saf.* **2019**, *174*, 137–145. [CrossRef] [PubMed]
39. Davidović, M.D.; Topalović, D.; Schneider, P.; Bartoňová, A.; Jovašević-Stojanović, M. Land use regression for particulate matter mapping: Data collection techniques, choice of predictor variables and possibilities for validation and improvement of maps. In Proceedings of the 5th WeBIOPATR Workshop & Conference, Belgrade, Serbia, 14–16 October 2015; Vinča Institute of Nuclear Sciences: Belgrade, Serbia, 2016; pp. 85–91.
40. Davidović, M.; Davidović, M.; Jovašević-Stojanović, M. Efficient tools for the creation and validation of LUR based maps. In Proceedings of the 6th WeBIOPATR 2017 Workshop and Conference, Belgrade, Serbia, 6–8 September 2017; Vinča Institute of Nuclear Sciences: Belgrade, Serbia, 2019; pp. 175–179.
41. Dmitrašinović, S.; Jovašević-Stojanović, M.; Radonić, J.; Davidović, M. Application of European $PM_{2.5}$ land use regression model on Novi Sad municipality, Serbia. In *Abstracts of Keynote Invited Lectures and Contributed Papers from the 9th WeBIOPATR 2023 Workshop and Conference, Belgrade, Serbia, 28 November–1 December 2023*; Vinča Institute of Nuclear Sciences: Belgrade, Serbia, 2023; p. 89.
42. Beelen, R.; Hoek, G.; Vienneau, D.; Eeftens, M.; Dimakopoulou, K.; Pedeli, X.; Tsai, M.Y.; Künzli, N.; Schikowski, T.; Marcon, A.; et al. Development of NO_2 and NOx Land Use Regression Models for Estimating Air Pollution Exposure in 36 Study Areas in Europe—The ESCAPE Project. *Atmos. Environ.* **2013**, *72*, 10–23. [CrossRef]
43. Habermann, M.; Billger, M.; Haeger-Eugensson, M. Land Use Regression as Method to Model Air Pollution. Previous Results for Gothenburg/Sweden. *Procedia Eng.* **2015**, *115*, 21–28. [CrossRef]
44. Liu, C.; Henderson, B.H.; Wang, D.; Yang, X.; Peng, Z.R. A Land Use Regression Application into Assessing Spatial Variation of Intra-Urban Fine Particulate Matter ($PM_{2.5}$) and Nitrogen Dioxide (NO_2) Concentrations in City of Shanghai, China. *Sci. Total Environ.* **2016**, *565*, 607–615. [CrossRef] [PubMed]
45. Shi, Y.; Bilal, M.; Ho, H.C.; Omar, A. Urbanization and Regional Air Pollution across South Asian Developing Countries—A Nationwide Land Use Regression for Ambient $PM_{2.5}$ Assessment in Pakistan. *Environ. Pollut.* **2020**, *266*, 115145. [CrossRef]
46. Hsu, W.T.; Ku, C.H.; Chen, M.J.; Da Wu, C.; Lung, S.C.C.; Chen, Y.C. Model Development and Validation of Personal Exposure to $PM_{2.5}$ among Urban Elders. *Environ. Pollut.* **2023**, *316*, 120538. [CrossRef]
47. Đorđević, T.; Tomić, N.; Tešić, D. Walkability and Bikeability for Sustainable Spatial Planning in the City of Novi Sad (Serbia). *Sustainability* **2023**, *15*, 3785. [CrossRef]
48. Statistical Office of the Republic of Serbia. Available online: https://www.stat.gov.rs/en-us/ (accessed on 12 February 2023).

49. Dmitrašinović, S.; Živković, M.; Jovanović, M.; Radonić, J.; Davidović, M. Traffic Intensity and Air Pollution before and during Lockdown in Novi Sad, Serbia. *Therm. Sci.* **2023**, *27*, 2333–2345. [CrossRef]
50. World Health Organization. *WHO Global Air Quality Guidelines. Particulate Matter ($PM_{2.5}$ and PM_{10}), Ozone, Nitrogen Dioxide, Sulfur Dioxide and Carbon Monoxide*; World Health Organization: Geneva, Switzerland, 2021; pp. 1–285. ISBN 9789240034228.
51. Davidović, M.; Dmitrašinović, S.; Jovanović, M.; Radonić, J.; Jovašević-Stojanović, M. Diurnal, Temporal and Spatial Variations of Main Air Pollutants before and during Emergency Lockdown in the City of Novi Sad (Serbia). *Appl. Sci.* **2021**, *11*, 1212. [CrossRef]
52. ESCAPE Exposure Assessment Manual Version 9, Version July 2010. Available online: http://www.escapeproject.eu/manuals/ESCAPE_Exposure-manualv9.pdf (accessed on 10 January 2020).
53. Brunekreef, B. Study Manual ESCAPE European Study of Cohorts for Air Pollution Effects. 2008. Available online: http://www.escapeproject.eu/manuals/ESCAPE-Study-manual_x007E_final.pdf (accessed on 15 April 2023).
54. Weissert, L.F.; Salmond, J.A.; Miskell, G.; Alavi-Shoshtari, M.; Williams, D.E. Development of a Microscale Land Use Regression Model for Predicting NO_2 Concentrations at a Heavy Trafficked Suburban Area in Auckland, NZ. *Sci. Total Environ.* **2018**, *619–620*, 112–119. [CrossRef]
55. Wang, M.; Beelen, R.; Basagana, X.; Becker, T.; Cesaroni, G.; de Hoogh, K.; Dedele, A.; Declercq, C.; Dimakopoulou, K.; Eeftens, M.; et al. Evaluation of Land Use Regression Models for NO_2 and Particulate Matter in 20 European Study Areas: The ESCAPE Project. *Environ. Sci. Technol.* **2013**, *47*, 4357–4364. [CrossRef]
56. Ghassoun, Y.; Löwner, M.O.; Weber, S. Wind Direction Related Parameters Improve the Performance of a Land Use Regression Model for Ultrafine Particles. *Atmos. Pollut. Res.* **2019**, *10*, 1180–1189. [CrossRef]
57. Zhou, Q.M.; Song, P.X.-K.; Thompson, M.E. Profiling Heteroscedasticity in Linear Regression Models. *Can. J. Stat.* **2014**, *43*, 358–377. [CrossRef]
58. Demir, S. Comparison of Normality Tests in Terms of Sample Sizes under Different Skewness and Kurtosis Coefficients. *Int. J. Assess. Tools Educ.* **2022**, *9*, 397–409. [CrossRef]
59. Ghasemi, A.; Zahediasl, S. Normality Tests for Statistical Analysis: A Guide for Non-Statisticians. *Int. J. Endocrinol. Metab.* **2012**, *10*, 486–489. [CrossRef]
60. Sundar, A.C. "From Pixels to Products: An Overview of Satellite Remote Sensing". NASA Earth Data Lecture. *You Tube*. 1 December 2021. Available online: https://youtu.be/ijjp1oyAmEE (accessed on 1 May 2024).
61. European Centre for Medium-Range Weather Forecasts (ECMWF). Available online: https://www.ecmwf.int/en/forecasts (accessed on 1 May 2024).
62. USGS Earth Resources Observation and Science (EROS) Center. Available online: https://lpdaac.usgs.gov/products/mcd19a2v061/ (accessed on 1 May 2024).
63. Liu, Y.; Sarnat, J.A.; Kilaru, V.; Jacob, D.J.; Koutrakis, P. Estimating ground-level $PM_{2.5}$ in the eastern United States using satellite remote sensing. *Environ. Sci. Technol.* **2005**, *39*, 3269–3278. [CrossRef]
64. Gupta, P.; Christopher, S.A. Particulate matter air quality assessment using integrated surface, satellite, and meteor ological products: Multiple regression approach. *J. Geophys. Res.* **2009**, *114*, D20205. [CrossRef]
65. Karimian, H.; Li, Q.; Wu, C.; Qi, Y.; Mo, Y.; Chen, G.; Zhang, X.; Sachdeva, S. Evaluation of different machine learning approaches to forecasting $PM_{2.5}$ mass concentrations. *Aerosol Air Qual. Res.* **2019**, *19*, 1400–1410. [CrossRef]
66. World Health Organization. *Health Impact of Ambient Air Pollution in Serbia a Call to Action*; World Health Organization Regional Office for Europe: København, Denmark, 2019; Available online: https://serbia.un.org/en/22141-health-impact-ambient-air-pollution-serbia-call-action (accessed on 1 April 2023).
67. Air Quality Plan in the Agglomeration of Novi Sad for the Period 2022–2026; City Administration for Environmental Protection Novi Sad: Novi Sad, Serbia. Available online: https://environovisad.rs/vesti/223 (accessed on 20 December 2022).
68. Kleut, D.; Davidović, M.; Dmitrašinović, S.; Živković, M.; Stojanović, D.; Budimir, M.; Lazović, I.; Jovašević-Stojanović, M.; Davidović, M. Air Quality Mobile Monitoring Campaign in Novi Sad Urban Area in Winter and Summer 2022. In Proceedings of the 22nd European Meeting on Environmental Chemistry, EMEC 22, Ljubljana, Slovenia, 5–8 December 2022.
69. Davidović, M.D.; Kleut, D.; de Vito, S.; Bartonova, A.; Jovašević-Stojanović, M. Mobile monitoring of urban ultrafine particles in Novi Sad, Serbia. In Proceedings of the 21st International Conference on Nucleation & Atmospheric Aerosols (ICNAA 2023), Brisbane, QLD, Australia, 26–30 June 2023.
70. He, B.; Heal, M.R.; Reis, S. Land-Use Regression Modelling of Intra-Urban Air Pollution Variation in China: Current Status and Future Needs. *Atmosphere* **2018**, *9*, 134. [CrossRef]
71. Shi, Y.; Lau, A.K.H.; Ng, E.; Ho, H.C.; Bilal, M. A Multiscale Land Use Regression Approach for Estimating Intraurban Spatial Variability of $PM_{2.5}$ Concentration by Integrating Multisource Datasets. *Int. J. Environ. Res. Public Health* **2022**, *19*, 321. [CrossRef]
72. Jeffrey, O.P. Modeling Spatiotemporal Patterns of $PM_{2.5}$ at the Sub-Neighborhood Scale Using Low-Cost Sensor Networks. Master's Thesis, Portland State University, Portland, OR, USA, 2020. [CrossRef]
73. Zhang, Y.; Cheng, H.; Huang, D.; Fu, C. High Temporal Resolution Land Use Regression Models with POI Characteristics of the $PM_{2.5}$ Distribution in Beijing, China. *Int. J. Environ. Res. Public Health* **2021**, *18*, 6143. [CrossRef]
74. Guo, B.; Wang, X.; Zhang, D.; Pei, L.; Zhang, D.; Wang, X. A Land Use Regression Application into Simulating Spatial Distribution Characteristics of Particulate Matter ($PM_{2.5}$) Concentration in City of Xi'an, China. *Pol. J. Environ. Stud.* **2020**, *29*, 4065–4076. [CrossRef]

75. Saucy, A.; Röösli, M.; Künzli, N.; Tsai, M.-Y.; Sieber, C.; Olaniyan, T.; Baatjies, R.; Jeebhay, M.; Davey, M.; Flückiger, B.; et al. Land Use Regression Modelling of Outdoor NO_2 and $PM_{2.5}$ Concentrations in Three Low Income Areas in the Western Cape Province, South Africa. *Int. J. Environ. Res. Public Health* **2018**, *15*, 1452. [CrossRef]
76. QGIS.org. QGIS Geographic Information System. QGIS Association. 2024. Available online: http://www.qgis.org (accessed on 15 January 2020).
77. Yang, W.; Jiang, X. Evaluating the Influence of Land Use and Land Cover Change on Fine Particulate Matter. *Sci. Rep.* **2021**, *11*, 17612. [CrossRef]
78. Shi, Y.; Ren, C.; Lau, K.K.L.; Ng, E. Investigating the Influence of Urban Land Use and Landscape Pattern on $PM_{2.5}$ Spatial Variation Using Mobile Monitoring and WUDAPT. *Landsc. Urban. Plan.* **2019**, *189*, 15–26. [CrossRef]
79. Xu, J.; Liu, M.; Chen, H. Spatial Heterogeneity of River Effects on $PM_{2.5}$ Pollutants in Waterfront Neighborhoods Based on Mobile Monitoring. *Atmos. Pollut. Res.* **2022**, *13*, 101539. [CrossRef]
80. Zhang, B.; Jiao, L.; Xu, G.; Zhao, S.; Tang, X.; Zhou, Y.; Gong, C. Influences of Wind and Precipitation on Different-Sized Particulate Matter Concentrations ($PM_{2.5}$, PM_{10}, $PM_{2.5–10}$). *Meteorol. Atmos. Phys.* **2018**, *130*, 383–392. [CrossRef]
81. Li, C.; Zhang, K.; Dai, Z.; Ma, Z.; Liu, X. Investigation of the Impact of Land-Use Distribution on $PM_{2.5}$ in Weifang: Seasonal Variations. *Int. J. Environ. Res. Public Health* **2020**, *17*, 5135. [CrossRef]
82. Yang, D.; Meng, F.; Liu, Y.; Dong, G.; Lu, D. Scale Effects and Regional Disparities of Land Use in Influencing $PM_{2.5}$ Concentrations: A Case Study in the Zhengzhou Metropolitan Area, China. *Land* **2022**, *11*, 1538. [CrossRef]
83. Olszowski, T. Influence of Individual Household Heating on $PM_{2.5}$ Concentration in a Rural Settlement. *Atmosphere* **2019**, *10*, 782. [CrossRef]
84. Askariyeh, M.H.; Venugopal, M.; Khreis, H.; Birt, A.; Zietsman, J. Near-Road Traffic-Related Air Pollution: Resuspended $PM_{2.5}$ from Highways and Arterials. *Int. J. Environ. Res. Public Health* **2020**, *17*, 2851. [CrossRef]
85. Amato, F.; Favez, O.; Pandolfi, M.; Alastuey, A.; Querol, X.; Moukhtar, S.; Bruge, B.; Verlhac, S.; Orza, J.A.G.; Bonnaire, N.; et al. Traffic Induced Particle Resuspension in Paris: Emission Factors and Source Contributions. *Atmos. Environ.* **2016**, *129*, 114–124. [CrossRef]
86. Wu, C.D.; Chen, Y.C.; Pan, W.C.; Zeng, Y.T.; Chen, M.J.; Guo, Y.L.; Lung, S.C.C. Land-Use Regression with Long-Term Satellite-Based Greenness Index and Culture-Specific Sources to Model $PM_{2.5}$ Spatial-Temporal Variability. *Environ. Pollut.* **2017**, *224*, 148–157. [CrossRef]
87. Yang, H.; Chen, W.; Liang, Z. Impact of Land Use on $PM_{2.5}$ Pollution in a Representative City of Middle China. *Int. J. Environ. Res. Public Health* **2017**, *14*, 462. [CrossRef]
88. Zhang, Z.; Wang, J.; Hart, J.E.; Laden, F.; Zhao, C.; Li, T.; Zheng, P.; Li, D.; Ye, Z.; Chen, K. National Scale Spatiotemporal Land-Use Regression Model for $PM_{2.5}$, PM_{10} and NO_2 Concentration in China. *Atmos. Environ.* **2018**, *192*, 48–54. [CrossRef]
89. Copernicus Land Monitoring Service. Available online: https://land.copernicus.eu/en/products/corine-land-cover/clc2018 (accessed on 1 December 2021).
90. OpenStreetMap Data Extracts. Available online: https://download.geofabrik-de/europe/serbia.html (accessed on 15 December 2021).
91. Lin, J.; Lin, Y.; Lin, S.; Dong, J. The Characteristic of Atmospheric Particulate Matter and the Influence Factors in Xiamen for Air Quality Management. *Front. Environ. Sci.* **2023**, *11*, 1220720. [CrossRef]

Disclaimer/Publisher's Note: The statements, opinions and data contained in all publications are solely those of the individual author(s) and contributor(s) and not of MDPI and/or the editor(s). MDPI and/or the editor(s) disclaim responsibility for any injury to people or property resulting from any ideas, methods, instructions or products referred to in the content.